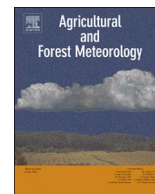




Contents lists available at ScienceDirect

Agricultural and Forest Meteorology

journal homepage: www.elsevier.com/locate/agrformet

Seasonal variation of source contributions to eddy-covariance CO₂ measurements in a mixed hardwood-conifer forest



JiHyun Kim^{a,b,*}, Taehee Hwang^b, Crystal L. Schaaf^c, Natascha Kljun^d, J. William Munger^e

^a Department of Earth & Environment, Boston University, Boston, MA, US

^b Department of Geography, Indiana University Bloomington, Bloomington, IN, US

^c School for the Environment, University of Massachusetts Boston, Boston, MA, US

^d Department of Geography, Swansea University, Swansea, UK

^e School of Engineering and Applied Sciences and Department of Earth and Planetary Sciences, Harvard University, Cambridge, MA, US

ARTICLE INFO

Keywords:

Eddy covariance flux measurement
Net ecosystem exchange
Spatial representativeness
Footprint model
Landsat EVI

ABSTRACT

Net ecosystem exchange (NEE) measurements using the eddy covariance technique have been widely used for calibration and evaluation of carbon flux estimates from terrestrial ecosystem models as well as for remote sensing-based estimates across various spatial and temporal scales. Therefore, it is vital to fully understand the land surface characteristics within the area contributing to these flux measurements (i.e. source area) when upscaling plot-scale tower measurements to regional-scale ecosystem estimates, especially in heterogeneous landscapes, such as mixed forests. We estimated the source area of a flux tower at a mixed forest (Harvard Forest in US) using a footprint model, and analyzed the spatial representativeness of the source area for the vegetation characteristics (density variation and magnitude) within the surrounding 1- and 1.5-km grid cells during two decades (1993–2011). Semi-variogram and window size analyses using 19 years of Landsat-retrieved enhanced vegetation index (EVI) confirmed that spatial heterogeneity within the 1-km grid cell has been gradually increasing for leaf-on periods. The overall prevailing source areas lay toward the southwest, yet there were considerable variations in the extents and the directions of the source areas. The source areas generally cover a large enough area to adequately represent the vegetation density magnitude and variation during both daytime and nighttime. We show that the variation in the daytime NEE during peak growing season should be more attributed to variations in the deciduous forest contribution within the source areas rather than the vegetation density. This study highlights the importance of taking account of the land cover variation within the source areas into gap-filling and upscaling procedures.

1. Introduction

Our understanding of the interactive dynamics between climate change and terrestrial ecosystem processes (Cao and Woodward, 1998; Finzi et al., 2011; Keenan et al., 2014; Nemani et al., 2003) has been remarkably progressed through the use of tower-based eddy covariance (EC) flux measurements (Baldocchi, 2003; Baldocchi et al., 1988; Falge et al., 2002; Law et al., 2002; Schmid et al., 2000). As unique *in-situ* and semi-continuous measurements, these flux tower data have been applied to a wide range of studies, such as statistical analysis for a single site or across multiple biomes (Keenan et al., 2013; Urbanski et al., 2007), and for correlation analysis with other biophysical attributes and processes (Davidson et al., 2006). These tower data have also been used for calibration and validation of mechanical ecosystem models and remote sensing-based estimates at various spatial resolutions (e.g., the

Moderate Resolution Imaging Spectrometer (MODIS) gross primary productivity (GPP) product at a 1-km resolution (Heinsch et al., 2006; Schwalm et al., 2010; Verma et al., 2015). The number of flux towers in the FLUXNET network (<http://fluxnet.ornl.gov/>) has increased rapidly, including about 846 sites as of November 2016. Mixed forests are some of the most common land covers in which flux towers have been set up (https://fluxnet.ornl.gov/site_list/IGBPLU/5). Several of the flux towers with the longest records, therefore the towers most frequently used in studies, are located in mixed forests such as Harvard Forest, MA, US (FLUXNET Site ID: US-Ha1, since 1991), Howland Forest, ME, US (US-Ho1,2,3, since 1995,1999, 2001), Morgan-Monroe State Forest, IN, US (US-MMS, since 1998), ON-Borden Mixed wood, Ontario, Canada (CA-Cbo, since 1995), Brasschaat, Belgium (BE-Bra, since 1996), and more.

Multiple factors have to be considered to determine whether the

* Corresponding author at: Department of Geography, Indiana University, Bloomington, IN, US.
E-mail address: jk237@iu.edu (J. Kim).

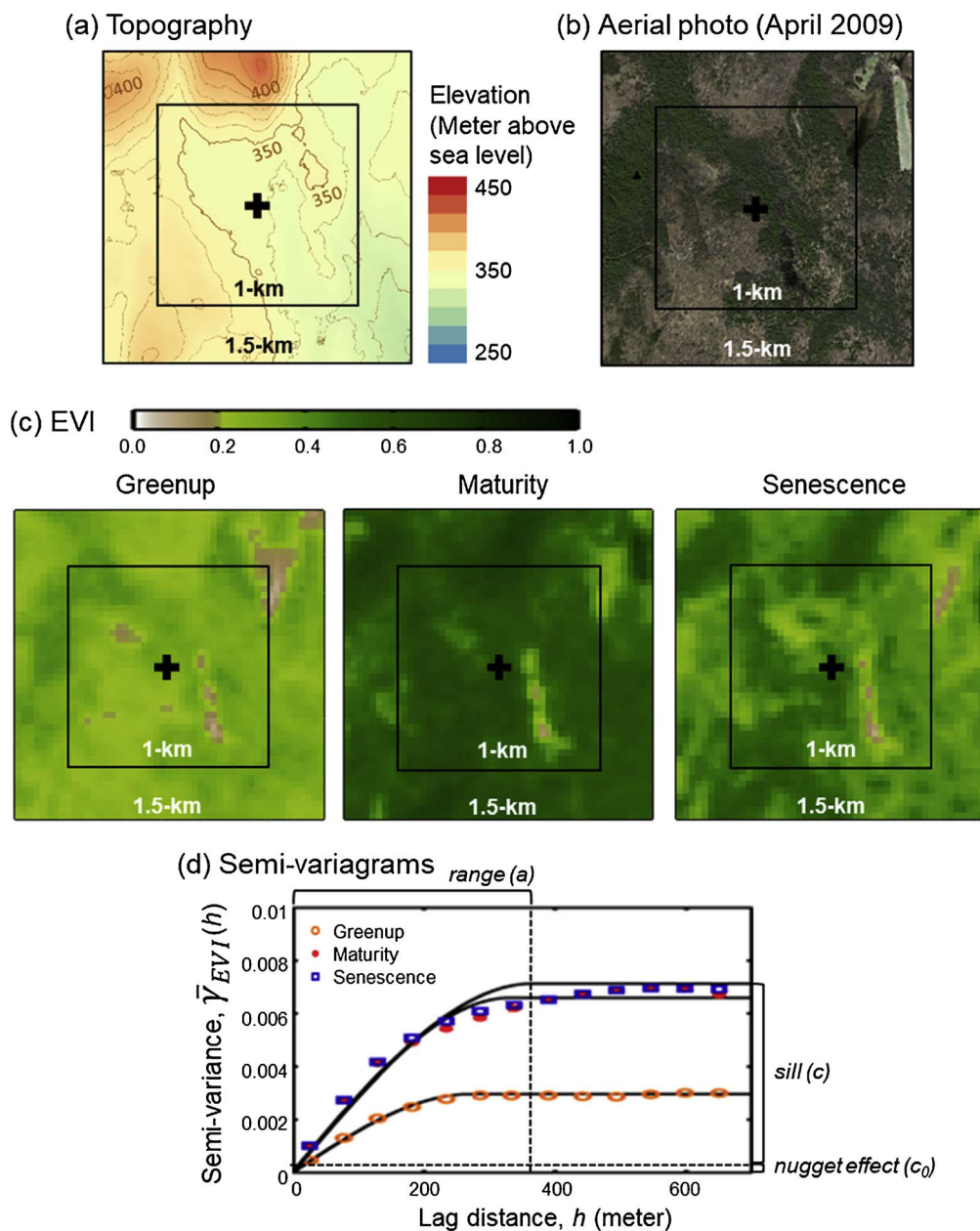


Fig. 1. (a) Topography of the surrounding area of the study tower (black cross). Elevation above sea level was retrieved from a LiDAR terrain file (accuracy of 5–35 cm; MassGIS: <http://www.mass.gov/>) (b) Aerial photo taken on April 2009 (30 cm resolution; MassGIS: <http://www.mass.gov/>) before the emergence of leaves on deciduous trees. (c) Enhanced vegetation index (EVI; Eq. (2)) maps retrieved from Landsat TM/ETM + scenes at each phenological stage: greenup (5/27/2008), maturity (8/31/2008) and senescence (10/18/2008). Details of the phenological stages are described in the data overview. (d) Schematic diagram of the semi-variogram estimators ($\bar{\gamma}_{EVI}(h)$) calculated from the EVI maps in (c) (orange circle, red dot, and blue square for greenup, maturity, and senescence stages, respectively), and the fitted isotropic spherical variogram models (black solid line), and ranges (dashed vertical lines in colors) (For interpretation of the references to color in this figure legend, the reader is referred to the web version of this article.)

upwind land surface measured by a flux tower (“source area”) adequately describes the characteristics of the surrounding ecosystem (“spatial representativeness”; Román et al., 2009; Schmid, 1997). This is especially critical in mixed forests, where temporally varying wind direction and atmospheric stability can change the source weight distribution of fluxes measured at a tower considerably over the heterogeneous land covers, resulting in a large degree of variations in the source area characteristics and therefore in the measured flux (Wehr and Saleska, 2015). This inevitable source area variability has long been recognized as one of the major uncertainties in flux measurements (Baldocchi, 2003). To understand and reduce this uncertainty, a number of studies have focused on developing a source weight function (“footprint”; Hsieh et al., 2000; Kljun et al., 2002, 2004; Kormann and Meixner, 2001; Schmid, 1994; van Ulden, 1978) and applying these

footprint models for the uncertainty analysis of flux measurements and also for ground-biometric sampling schemes (Amiro, 1998; Chasmer et al., 2011; Griebel et al., 2016; Novick et al., 2014; Oishi et al., 2008; Stoy et al., 2006; Xu et al., 2017). There are also ongoing efforts to standardize the source area estimation at the network levels (Menzer et al., 2015, 2014). However, as of yet, most studies of mixed forests have not fully considered the temporal variations in source areas, but instead have only approximated a fixed area (Turner et al., 2003; Verma et al., 2015) or simply rejected some flux data solely based on wind direction (Daley et al., 2007; Phillips et al., 2010). Such wind-direction based filtering schemes sometimes leave only 25% of the total data deemed as appropriate for further analysis (Hadley & Schedlbauer, 2002; Stoy et al., 2006), yet still leaves questions about the representativeness of the flux data for large-scale applications.

Furthermore, even those studies that assessed the spatial representativeness of flux measurements for the surrounding landscape using footprint models have usually only performed this assessment for a limited time period, such as for a single season or for only a few years, mainly due to the high computational costs (Chen et al., 2012; Göckede et al., 2008; Kim et al., 2006; Schmid and Lloyd, 1999). In a mixed forest, however, the spatial representativeness of source areas may experience significant seasonal variations, depending on vegetation types and their spatial distributions around the tower. For example, the phenological stage of deciduous trees (greenup, maturity, senescence, and dormancy onsets) can be a primary factor that transforms the entire surrounding landscape and drives the seasonal cycle of flux measurements. Román et al. (2009) showed that the representativeness of tower-based albedo measurements (note: a tower albedometer has a fixed viewing angle) for the evaluation of moderate resolution satellite-derived albedo products is largely dependent on the timing of greenup of deciduous trees, the distribution of conifer trees within the source area, and gridded resolutions of the satellite products (~1-km and 1.5-km). The intrinsic physiological differences among vegetation functional types also contribute to the spatial variations in biophysical attributes over the landscape. Tian et al. (2002) described that 76% of total variance in leaf area index (LAI) within a 15×13 km area in a mixed forest is mostly governed by the spatial variation of vegetation functional types. There are also additional factors driving interannual and long-term changes in spatial landscape characteristics of mixed forests, such as the different sensitivities to interannual climate variability (Welp et al., 2007) and changes in vegetation types and distributions due to ongoing climate change (Battles et al., 2007). Therefore, it is critical to understand long-term representativeness of source areas when interpreting flux measurements in mixed forests and when using these measurements to evaluate ecosystem models and remote sensing-based models across different temporal and spatial scales.

In this study, first we calculate hourly source weights for a flux tower in a mixed forest for 19 years (1993–2011). Based on these source weight estimates, we then examine the representativeness of the source area for the surrounding vegetation characteristics (density magnitude and variation) at moderate-spatial resolutions (1-km and 1.5-km) during daytime and nighttime, separately, for each phenological stage. Finally, we investigate how much of the variation in the measured flux can be attributed to vegetation density and land cover based on their footprint-weighted contributions.

2. Materials and methods

2.1. Study site

The Environmental Measurement Site tower (42.537755°N, 72.171478°W; US-Ha1) is located in the Harvard Forest Long Term Ecological Research (LTER) site in Petersham, Massachusetts. The topography in this area is relatively moderate, with elevation ranging from 320 to 380 meters above sea level (Fig. 1a). The forest has a cool and moist temperate climate with annual mean temperature of about 8.5 °C (20 °C in July and -7 °C in January) and annual total

precipitation of approximately 1100 mm, with winds primarily from southwest and northwest (<http://harvardforest.fas.harvard.edu/research/HF-tract>). The forested landscape is dominated by several tree species, including northern red oak (*Quercus rubra*), red maple (*Acer rubrum*), eastern hemlock (*Tsuga canadensis*), white pine (*Pinus strobus*), and black birch (*Betula lenta*) (Urbanski et al., 2007). Mean ages of northern red oak and eastern hemlock are about 97 and 145 years, respectively (Belmecheri et al., 2014). Canopy height is at about 20–24 meters (Goulden et al., 1996; Wang et al., 2011). Basal area is about $33.5 \text{ m}^2 \text{ ha}^{-1}$ (Munger and Wofsy, 1999a). Deciduous trees occupy the southwestern area from the tower with scattered patches of coniferous trees (Fig. 1b). In mid-September of 1999, beaver activity caused a flood on the northwest side of the tower, developing a small woody wetland (Savage and Davidson, 2001; Urbanski et al., 2007). Additional beaver activity temporarily flooded an area along the Bigelow brook on the southeast side of the tower in recent years. This forest has been experiencing a hemlock woolly adelgid infestation since late 2000s (Orwig et al., 2008), but significant hemlock mortality was not yet been observed close to the tower over the study period (until 2011; Kim et al., 2017).

The tower measurements, which began in Oct 1991, provide the longest continuous set of flux measurements in the US (Baldocchi et al., 1988; Goulden et al., 1996; Urbanski et al., 2007). Ground transects were established in 1993 along the prevailing wind directions, southwest and northwest (220–254 and 291–325 compass degrees). Since 1995, biometric and abiotic data has been collected along these transects 20–30 times a year, which include soil samples (water content, temperature and respiration), biomass measurements (leaf area index, litterfall and woody debris), and below-canopy microclimate observations (air temperature and solar radiation). Datasets are publicly available on the Harvard Forest LTER, AmeriFlux and FLUXNET websites (<http://harvardforest.fas.harvard.edu>; <http://ameriflux.lbl.gov>; Munger and Wofsy, 1999a,b).

2.2. Data overview

We used the hourly quality-checked NEE data ($\text{g C m}^{-2} \text{ s}^{-1}$) of the FLUXNET2015 dataset (<http://fluxnet.fluxdata.org/data/fluxnet2015-dataset/>); data quality assessment processes are described in Pastorello et al. (2014). Micrometeorological and energy flux data such as friction velocity (u^*), wind direction (α), the standard deviations and covariances of wind components ($\sigma_u, \sigma_v, \sigma_w, \overline{u'v'}, \overline{u'w'}$), air temperature (T_{air}), photosynthetically active radiation (PAR), vapor pressure deficit (VPD), and sensible heat flux (H), were acquired at the above-canopy 29 m point of the tower as was the NEE data (Munger and Wofsy, 1999b; additional data upon request: tower PI J. William Munger). Only directly measured NEE data was used to avoid any uncertainty or bias in gap-filling procedures, and the u^* threshold was set to 20 cm s^{-1} (Urbanski et al., 2007).

At the study site, visual observations of the percentage of leaf size (from April through June) and the percentage of colored leaves on a tree (from September through November) have been performed at every 3–7 days since 1990 (O'Keefe, 2000). We used the observation

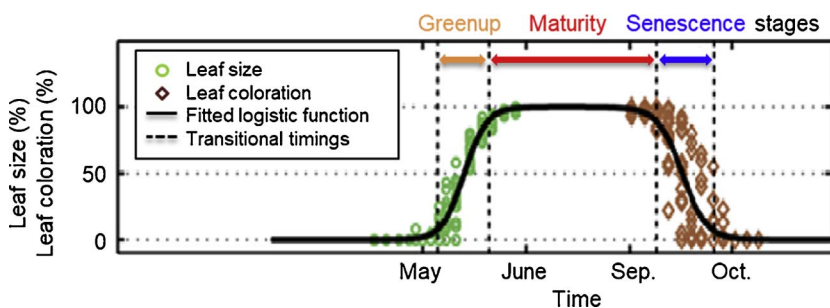


Fig. 2. Schematic diagram of estimating phenological stages. Leaf size and coloration data (green circles and brown diamonds) are based on ground-based visual observations (O'Keefe, 2000; data shown here is of 2008). A logistic function (Eq. (1)) is fitted to the indices for leaf size and coloration data, respectively (black solid line). Phenological stages (greenup, maturity, and senescence) are the periods between the phenological transitional timings (the dates when the curvature of the fitted function have the greatest changes; vertical dashed line).

data of the two dominant deciduous species (northern red oak and red maple) from 1993 to 2011 to determine the phenological stages of the deciduous broadleaf forest (DBF). A piecewise logistic function (Eq. (1) and Fig. 2) was fitted to leaf size and coloration data, respectively, for each year (Fig. S2). The dates when the curvature of the fitted function has the greatest changes were defined as four phenological transitional dates: greenup, maturity, senescence, and dormancy onsets (Hwang et al., 2011; Zhang et al., 2003).

$$I(t) = \frac{1}{1 + e^{a+tb}} \quad (1)$$

where $I(t)$ is index from leaf data, t is the day of year. The fitting coefficients (a and b) were estimated using a nonlinear regression (*nlinfit*, Matlab R2013a, MathWorks Inc., Natick, MA). The three phenological stages (i.e. greenup, maturity, and senescence) are the periods between the phenological transitional dates (Fig. 2).

We collected all available Landsat-5 Thematic Mapper (TM) and Landsat-7 Enhanced Thematic Mapper Plus (ETM +) scenes from 1993 to 2011 (<http://earthexplorer.usgs.gov/>; Landsat-7 during 1999–2003). Landsat scenes have high spatial- and moderate temporal-resolutions (30 m and 16 day overpass cycle), and they cover the entire study period, which facilitates efficient and consistent assessments of the landscape heterogeneity at the study site. We retrieved surface reflectance data on only cloud-free days using the Landsat Ecosystem Disturbance Adaptive Processing System (LEDAPS; Masek et al., 2006). In this study, we used the enhanced vegetation index (EVI; Eq. (2)) as an indicator of vegetation density (e.g. LAI) because EVI is more sensitive to LAI in a closed canopy forest than other vegetation indices (Gao, 2000; Huete et al., 2002).

$$EVI = G \frac{\rho_{nir} - \rho_{red}}{\rho_{nir} + C_1 \rho_{red} - C_2 \rho_{blue} + L} \quad (2)$$

where ρ is the surface reflectance in near-infrared, red, and blue bands (ρ_{nir} , ρ_{red} , and ρ_{blue}), C_1 and C_2 are the aerosol resistance coefficients, G is gain factor, and L is the canopy background adjustment. The coefficients are set as follows: $L = 1$, $C_1 = 6$, $C_2 = 7.5$, and $G = 2.5$ (Huete et al., 2002).

The land cover in this study is based on three National Land Cover Dataset products at five-year intervals (NLCD 2001/2006/2011; <http://www.mrlc.gov/>). The NLCD 1992 was not included in this study because the land cover definitions in the NLCD 1992 are different from those defined in the others (Trotter et al., 2013). These NLCD products were derived from Landsat imagery, therefore having a spatial resolution of 30 m.

2.3. Footprint model and flux source attributes

We calculated the hourly source weights (φ) for the directly-measured and quality-checked hourly NEE data from 1993 to 2011 using the Flux Footprint Prediction (FFP) model (Kljun et al., 2015; <http://footprint.kljun.net>). For the FFP model, the sensor height parameter (z_m) was set to the instrument height minus the zero-plane displacement height ($d = 2/3$ times the canopy height; Stull, 1988). The sonic anemometer is mounted at 29 m on the tower, and the canopy height was set to 21 m in this study. Manual observations in 1992 when the tower was installed (Goulden et al., 1996) and airborne LiDAR measurements in 2003 (Fig. S1; Park et al., 2014; Wang et al., 2011) show no significant differences outside their respective uncertainty and spatial variability. Further input parameters, such the standard deviation of lateral velocity fluctuations (σ_v), the friction velocity (u_*), and the wind direction were all directly derived from the EC data. The surface roughness length (z_0) was set to 1.6 m for both deciduous and coniferous canopies at the study site (Hadley and Schedlbauer, 2002; Wu et al., 2015). The planetary boundary layer (h) was calculated depending on the atmospheric stability, such as stable (Obukhov length, $L > 0$), neutral ($L \rightarrow \infty$), and convective ($L < 0$) conditions (Kljun

et al., 2015). It should be noted that the FFP model assumes the upwind domain is spatially homogeneous, a condition that is complied with at the study site where the topography is moderate (elevation variation less than 60 m) and the canopy height distribution is mostly even (Fig. S1; standard deviation (SD) of 2.6 m within the 500-m grid cell; Wang et al., 2011).

In this study, we limited the extent of an source area at the 80% source weight (φ_{80}) as the uncertainty of any footprint model increases for larger extents (Kljun et al., 2015). We then calculated the geometric mean of the along-wind distance from the tower and the crosswind distance at the peak location.

We focused on two flux source attributes: vegetation density and land cover type. We calculated the 1-km grid cell mean EVI (\overline{EVI}_{1km}) and footprint-weighted EVI ($EVI_{\varphi_{80}}$ in Eq. (3); Kim et al., 2006).

$$EVI_{\varphi_{80}} = \sum_{i=1}^{N_{\varphi_{80}}} \varphi_{80,i} EVI_i \quad (3)$$

where i designates one pixel, and $\varphi_{80,i}$ and EVI_i are the source weight (φ_{80}) and the EVI value at i -pixel. $N_{\varphi_{80}}$ refers the total number of pixels within the source area. The relative contribution of each land cover to flux measurements, i.e., the footprint-weighted proportion of each land cover ($P_{\varphi_{80}}$; Eq. (4)), was calculated by summing and normalizing the source weights of the respective land cover (Chen et al., 2013).

$$P_{\varphi_{80},k} = \frac{\sum_{i=1}^{N_k} \varphi_{80,i}}{\sum_{i=1}^{N_{\varphi_{80}}} \varphi_{80,i}} \times 100 \quad (4)$$

where N_k refers to the total number of pixels for each land cover (k) within the source area. Due to the limited availability of the NLCD for the early 1990s, we did not include the first 6 years of the study period (1993–1998), and partitioned the remaining study periods to situate each NLCD at the center year: NLCD 2001 for the 5 years from 1999 to 2003, NLCD 2006 from 2004 to 2008, and NLCD 2011 for the other 3 years (2009–2011).

2.4. Quantification of spatial heterogeneity

The semi-variogram model has been recognized as one of the most efficient tools to describe spatial heterogeneity and autocorrelation in sample measurements (Carroll and Cressie, 1996; Curran, 1988; Davis, 1986; Woodcock et al., 1988a), ranging from abiotic phenomena (e.g. temperature and precipitation; Haylock et al. 2008) to biophysical attributes (e.g. surface vegetation albedo; Román et al. 2009). The semi-variance is defined as the average of the half variances of $N(h)$ pairs of observations at an interval distance (lag distance) of h (Curran, 1988). The semi-variance estimator ($\overline{\gamma}_{EVI}(h)$; Eq. (5)) here was calculated as half the average-squared-difference between EVI values at a pair of pixels separated by a distance h .

$$\overline{\gamma}_{EVI}(h) = \frac{\sum_i^{N(h)} \gamma_i(h)}{N(h)} = \frac{\sum_i^{N(h)} (Z_{xi} - Z_{xi+h})^2}{2N(h)} \quad (5)$$

where Z_{xi} is the EVI value at a pixel (x_i), and Z_{xi+h} is the EVI value at a pixel (x_{i+h}) within a lag distance h , therefore a multiple of 30 m in this study which is the nominal resolution of Landsat scenes. The maximum lag distance for a 1-km grid cell is 690 m, half of the length of the diagonal of the 1-km boundary. The isotropic spherical variogram model in Eq. (6) (Matheron 1963) was fitted to the semi-variance estimators to obtain the variogram parameters: *nugget effect* (c_0), *sill* (c), and *range* (a) in Fig. 1d.

$$\gamma_{SPH}(h) = \begin{cases} c_0 + c \left(1.5 \left(\frac{h}{a} \right) - 0.5 \left(\frac{h}{a} \right)^3 \right), & 0 \leq h < a \\ c_0 + c, & h \geq a \end{cases} \quad (6)$$

The *nugget effect* is an estimation of the variance at a lag distance of zero, indicating microscale variability within the smallest sampling distance, uncertainty in the measurements, or combination of both

factors (Noréus et al., 1997). The *sill* represents a horizontal asymptote value of the variogram model, reflecting absolute magnitude of heterogeneity within the study grid cell (1-km and 1.5-km in this study). The variogram reaches the *sill* at the lag distance, *range*, beyond which there is no further spatial covariance between biophysical properties. We quantified the spatial variation in the vegetation density at moderate resolutions (1 and 1.5-km) with the semi-variogram model using the Landsat-retrieved EVI from 1993 to 2011 (Román et al., 2009; Susaki et al., 2007). Examples of the EVI maps retrieved from the Landsat scenes of the 1-km and 1.5-km grid cells centered at the tower during greenup, maturity, and senescence stages are shown in Fig. 1c.

While a semi-variogram analysis provides information about the spatial variation of the entire study grid cell, spatial heterogeneity surrounding the tower can be assessed with a window size analysis (Kim et al., 2006). The vegetation density index (EVI in this study) within a window centered at the tower was averaged (\overline{EVI}) for increasing size of the window (to a square window). The window-averaged EVI difference from the 1-km grid cell mean EVI (ΔEVI_i ; Eq. (7)) was calculated as the window width increased

$$\Delta EVI_i = \overline{EVI}_i - \overline{EVI}_{1km} \quad (7)$$

while \overline{EVI}_{1km} refers to the 1-km grid cell mean EVI, and the size of window (*i*) increases by multiples of 30 m, the nominal resolution of Landsat scenes: *i* = 30, 90, ..., 990 m (approximate width of \overline{EVI}_{1km}), ..., 1500 m.

2.5. Significant factors of flux variation

We examined how much variation in the hourly NEE could be accounted for by the flux source attributes (i.e. vegetation density and land cover type) during each phenological stage. To minimize the confounding effects of the weather and source weight distributions, the hourly NEE data was classified into a series of classes depending on its meteorological condition (Wu et al., 2013). Each meteorological class is a combination of temperature (equal intervals of 10 °C), PAR (50 $\mu\text{mol m}^{-2} \text{s}^{-1}$), and VPD (100 Pa) classes, resulting in 8405 in total.

We applied an ordinary least squares (OLS) regression between NEE and the vegetation density measure ($EVI_{\varphi 80}$) for the meteorological classes when at least 10 observations of both EVI and NEE on the same day with EVI are available (Wu et al., 2013). We also examined the correlation between NEE and \overline{EVI}_{1km} for a meteorological condition when each of temperature, VPD, and PAR was beyond the 75th percentile value of its cumulative distribution function (Fig. S4). We then examined the correlation of the land cover type with a multiple linear regression between NEE and the footprint-weighted land cover proportions ($P_{\varphi 80}$) for each meteorological class. We assumed that the measured NEE were only contributed from the vegetated land covers, therefore the intercept was forced to zero (Hutjes et al., 2010).

$$NEE = \sum_{k=1}^n f_k P_{\varphi 80,k} \quad (8)$$

where *n* is the number of land covers (*n* = 4) and f_k is the coefficient for land cover *k* (deciduous broadleaf forest (DBF), evergreen needleleaf forest (ENF), mixed forest (MF), and woody wetland). A negative f_k indicates a carbon uptake rate per unit land cover proportion ($\text{g C m}^{-2} \text{s}^{-1} \%^{-1}$) as a negative NEE means an uptake from the atmosphere in this study. This analysis was carried out for 13 years (1999–2011) due to the limited availability of the NLCD products. The adjusted coefficient of determination (R_{adj}^2) of the OLS regression (against $EVI_{\varphi 80}$) and the R_{adj}^2 of the multiple linear regression (against $P_{\varphi 80}$) was then compared separately for daytime (PAR > 50 $\mu\text{mol m}^{-2} \text{s}^{-1}$) and nighttime during each phenological stage.

3. Results

3.1. Phenological onset timings and stages

The phenological transitional timings have varied every year (Fig. S3), and the greenup stage was from May 10 to June 5, the maturity stage (peak growing season) from June 5 to September 17, and the senescence stage from September 17 to October 19 on average from 1993 to 2011. Growing season was defined from the greenup onset to the dormancy onset, therefore from May 10 to October 19 on average.

3.2. Footprint extent and distribution variation

At the tower, the prevailing wind directions over the study period were mostly southwest and northwest during both the daytime and nighttime (Fig. S5a; Davidson et al., 2006; Urbanski et al., 2007), but there were variations in the wind speed frequency distribution between the phenological stages (Fig. S5b). Strong northwesterly and westerly winds are noticeable during the greenup and senescence stages (Fig. S5b). Prevailing wind direction and frequency are of high impact to the source weight distribution, therefore the dominant orientation of source areas were mostly toward the southwest (source weight peak locations at 212–236°; Fig. S6) while there were more variations during the greenup and senescence stages. Furthermore, there was a noticeable difference in the source area sizes between the daytime and nighttime (Fig. 3) as source areas had larger extent with larger variation due to the stable atmospheric condition during nighttime (Fig. S6). The geometric mean of along-wind and crosswind distances was mostly different between the daytime and nighttime, while rather similar across phenological stages (163.5–190.6 with standard deviation (SD) of 55.8–70.4 m during the daytime, and 298.9–221.8 with SD of 128.8–159.6 m during the nighttime). The distance between the tower and source weight peak location was also smaller and less variable during the daytime than during the nighttime, 39.4 ± 3.4 and 58.3 ± 30.4 m, respectively (Fig. S6).

The 1-km grid cell around the tower from the NLCD 2001 primarily consisted of DBF (Fig. S8). The transition from the NLCD 2001 to the NLCD 2006 shows that there was a slight expansion of the wetland on the northwest side of the tower. There were considerable changes from the NLCD 2006 to the NLCD 2011 due to flooding and draining of the wetlands on the northwest and southeast sides of the tower. The 1-km grid cell consisted of 47.5% of DBF, 22.1% of ENF, 15.0% of mixed forest, and 10.9% of woody wetland in the NLCD 2001, while it consisted of 47.7% of DBF, 16.2% of ENF, 14.8% of mixed forest, and 15.3% of woody wetland in the NLCD 2011. The footprint-weighted land cover proportions ($P_{\varphi 80}$; Eq. (4)) were quite different for the daytime and nighttime, relatively similar across the phenological stages (Fig. 4), due to the combined effect of the heterogeneous landscape and the variations in source areas. During the daytime, DBF is the most dominant land cover contributing about 78.3% of measured fluxes on average (SD of 19.0%), which is about 30% higher than the nominal proportion of DBF within the 1-km grid cell in the NLCD. During the nighttime, the $P_{\varphi 80}$ of DBF was slightly lower and more variable than during the daytime, at about 71.3% on average (SD of 25.1%). ENF contributed 14.5% and 19.0% during the daytime and nighttime, respectively (SD of 15.9–19.1%). The $P_{\varphi 80}$ of other covers (mixed forest, woody wetland, and open space area) were less than 5%, respectively (Fig. 4).

3.3. Spatial heterogeneity of the study site

The *nugget effect* values (Fig. 5a) (indicators of measurement errors or microstructures within the grid cells) were primarily driven by canopy closure (i.e. phenological stage), rather than long-term landscape changes. The *nugget effect* values of the 1-km grid cell were higher than 0.0005 before the entire growing seasons started, and the values

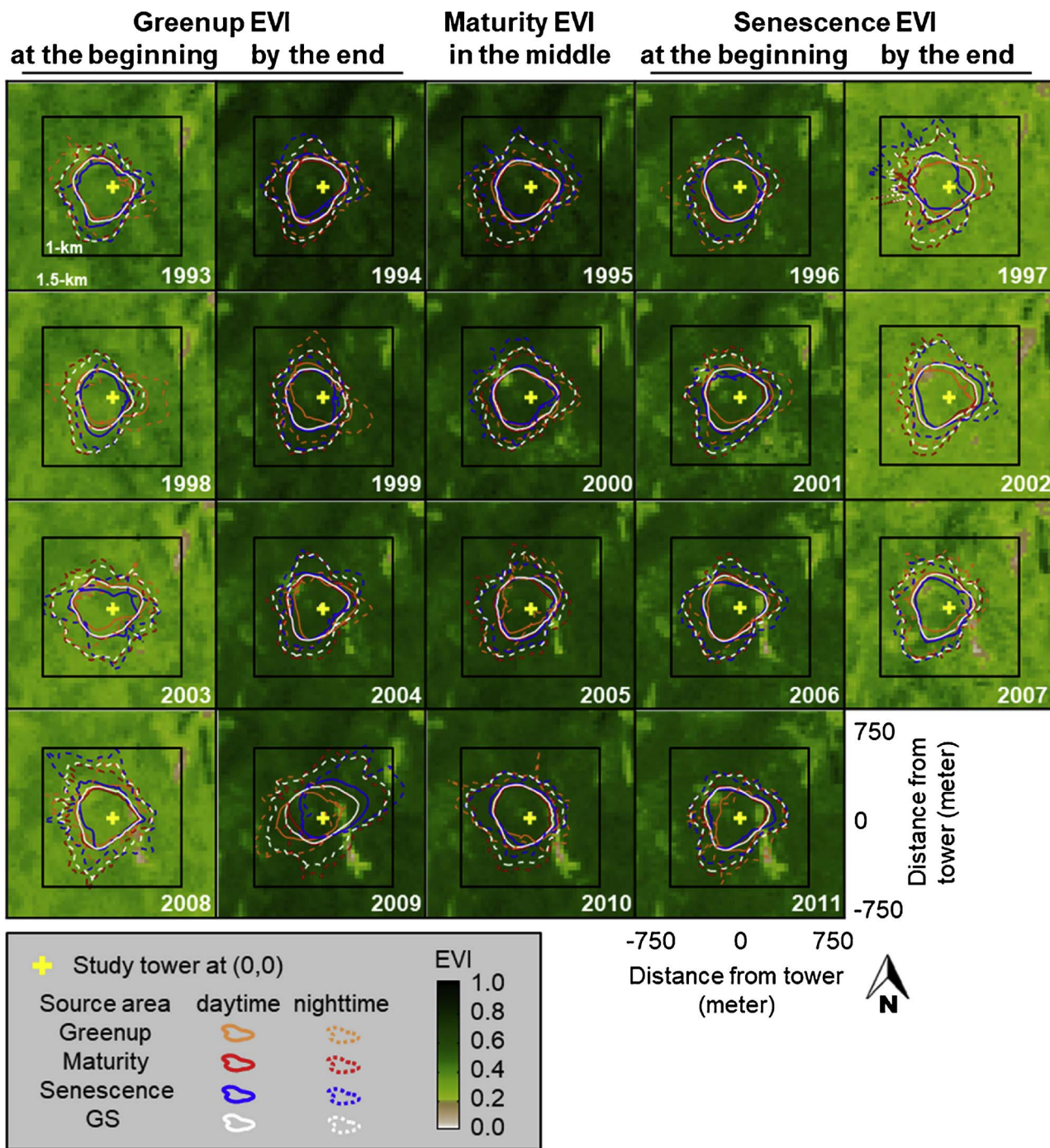


Fig. 3. Footprint climatology (i.e., an aggregation of source areas) during the daytime and nighttime (solid and dashed contours, respectively) during each phenological stage (greenup, maturity, senescence, and growing season, GS) from 1993 to 2011 overlaid on 1.5-km grid cell EVI maps centered at the study tower (yellow cross). EVI maps during the greenup stage are shown in the first and second columns, maturity stage in the third column, and senescence stage in the fourth and fifth columns.

substantially declined by the beginning of the greenup stages. As the forest canopy at the sub-pixel scale was almost completely closed during the entire growing seasons, there were almost no sub-pixel scale variations (*nugget effect* values ~ 0), although the values started to increase at the end of the senescence stages as open canopy gaps started to contribute to increased microstructures over the study site. The non-vegetated area and woody wetlands at the northeast corner of the 1.5-km grid cell (Fig. 1b) caused a high level of *nugget effect* values during the maturity and senescence stages (Woodcock et al., 1988b).

There were also seasonal and long-term changes in the *sill* values (the overall changes in the spatial heterogeneity within the study grid cells) (Figs. 5b and S7a). In the early 1990s, the *sill* values of 1-km grid

cell were low and nearly constant (around 0.002) throughout the entire growing seasons. Because of the wetland on the northwest side of the tower (Fig. S7b), the spatial variations started to increase during the maturity stage of 2001, although these variations consistently returned to a low level by the end of each senescence stage. The other wetland on the southeast side of the tower has contributed to the gradual increase in spatial variations within the 1-km grid cell during the maturity stages for the last few years (Figs. 5b and S7a). The flooding and draining of those two wetlands did not have any significant impact on the spatial variation of the 1.5-km grid cell which was already heterogeneous before the wetland expansion (Fig. 5b).

The *range* values (the distance limit within which the surface

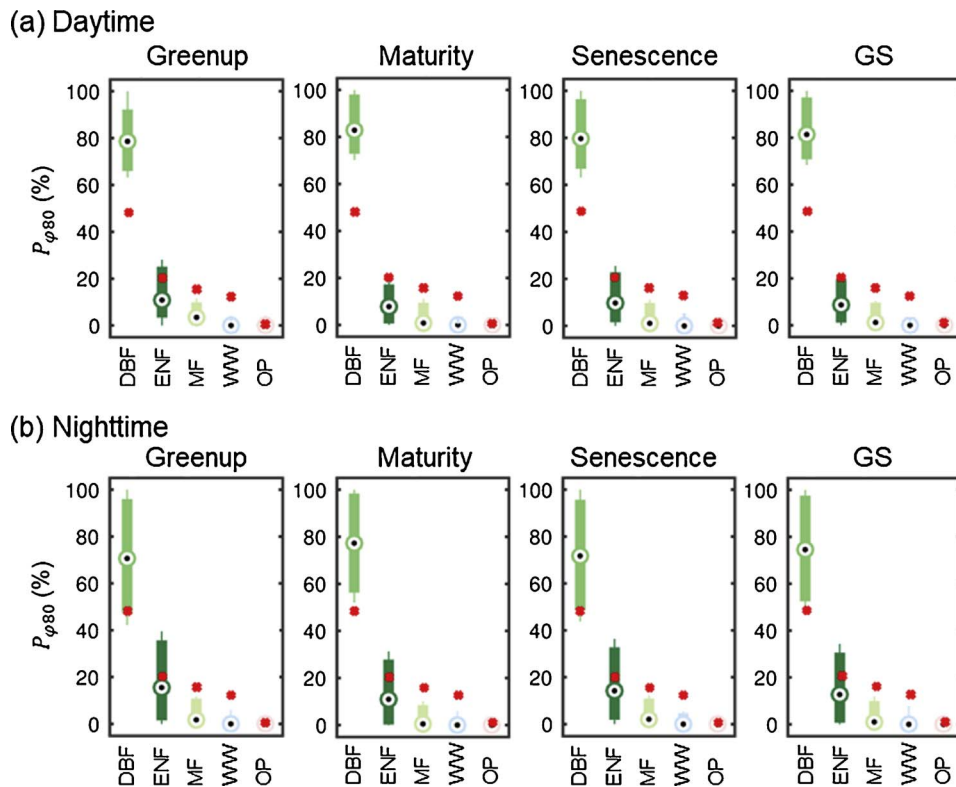


Fig. 4. The footprint-weighted proportions ($P_{\phi 80}$; Eq. (4)) of each land cover (deciduous broadleaf forest (DBF), evergreen needleleaf forest (ENF), mixed forest (MF), woody wetland (WW), and open space area (OP) during the daytime (a) and the nighttime (b) during greenup, maturity, and senescence stages, and during entire growing season (GS) from 1999 to 2011. The box shows upper and lower quartile range of the $P_{\phi 80}$ and the black dots represent the median values. The average value of the nominal proportions of each land cover within the 1-km grid cell in the NLCD products is marked as a red dot. The hourly $P_{\phi 80}$ during each phenological stage can be found in Fig. S9.

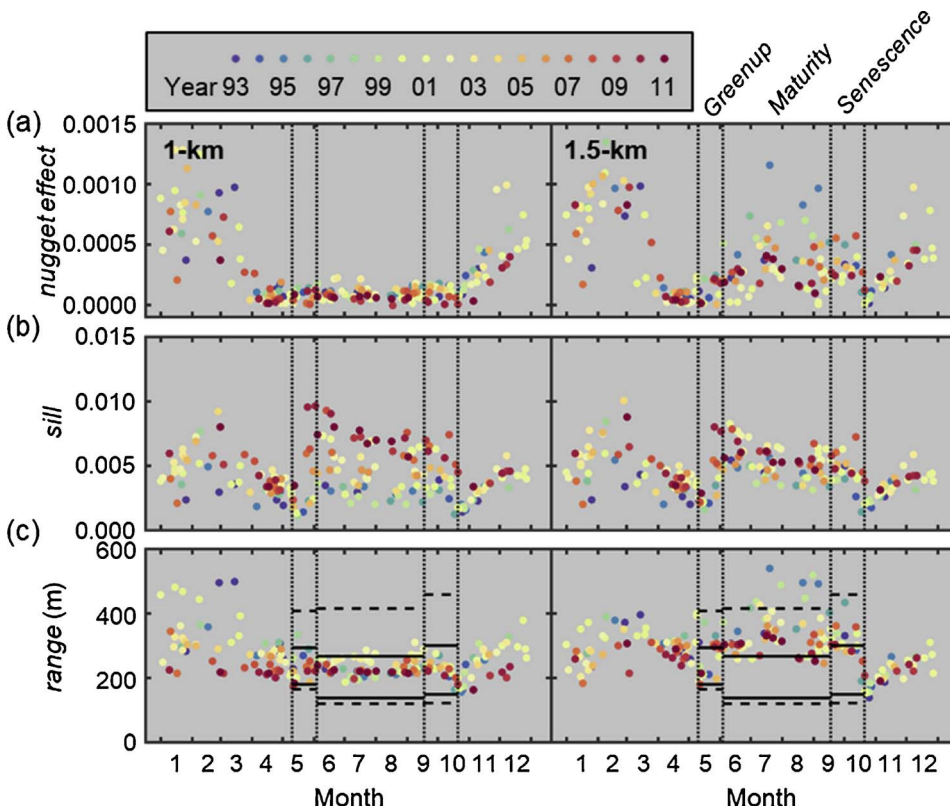


Fig. 5. Semi-variogram parameters, the *nugget effect* (a), *sill* (b), and *range* (c), derived from EVI within 1-km (left panels) and 1.5-km (right panels) grid cells from 1993 to 2011 (in different colors). One standard deviation of the geometric mean value of along-wind and crosswind distances during the daytime and nighttime (horizontal solid and dashed lines, respectively) is presented in the *range* plot (c) during each phenological stage (greenup, maturity and senescence).

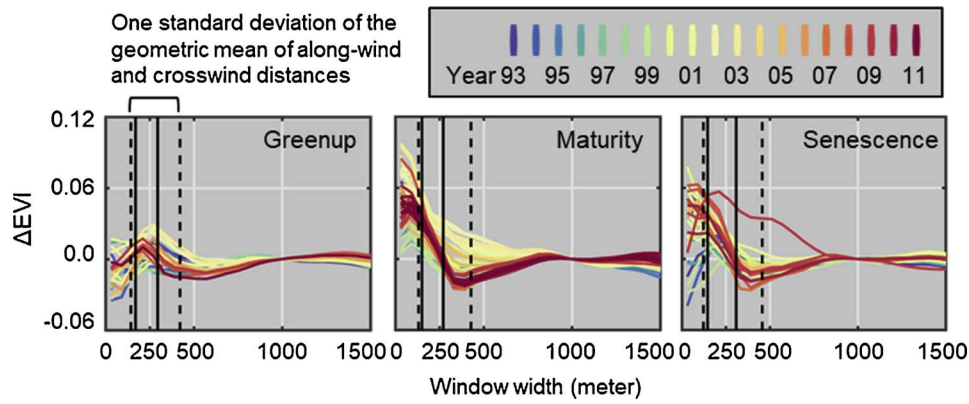


Fig. 6. The window-averaged EVI difference from the 1-km grid cell mean EVI (ΔEVI ; Eq. (7)) between 1993 and 2011 (in different colors) during greenup, maturity, and senescence stages, respectively. One standard deviation of the geometric mean of along-wind and crosswind distances during the daytime and nighttime for each phenological stage is presented in vertical solid and dashed lines, respectively.

variations are auto-correlated) within the 1-km grid cell were mostly constant during the entire growing seasons (Fig. 5c). Most of the range values (280 m, 265 m, and 250 m on average during the greenup, maturity, and senescence stages, respectively) were within one standard deviation of the geometric mean of along-wind and crosswind distances during both the daytime and nighttime. The range values of the 1.5-km grid cell were higher than those of the 1-km grid cell due to the non-vegetated area at the northeastern corner (Fig. 1b).

ΔEVI , the difference between the window-averaged EVI and 1-km grid cell averaged EVI (i.e., the spatial heterogeneity of the tower surrounding area), was mostly negative around the tower during the greenup stage when the canopy of deciduous trees has not yet fully emerged yet (Fig. 6). The ΔEVI slightly increased at a window width of 250 m, including the conifer trees located on the northwest, northeast, and southeast sides of the tower (Fig. 1b), and then gradually converged to zero around a 1-km window width. Overall, the variations in the ΔEVI during the greenup stage were relatively small (less than 0.05) regardless of window widths. Meanwhile, the ΔEVI during the maturity and senescence stages revealed strong spatial heterogeneity around the tower. The ΔEVI values were higher than zero during the maturity stage (i.e. the averaged EVI around the tower was up to 16% higher than the magnitude of \overline{EVI}_{1km}), and then gradually converged to zero at the window widths of 700 and 500 m during the maturity and senescence stages, respectively (Fig. 6). The development of the southeast-side wetland has gradually decreased the ΔEVI at a window width between 250 and 500 m during the maturity stage.

3.4. Significance of flux source attributes

Over an entire growing season, the measured NEE was significantly correlated with both vegetation density measures ($R_{adj}^2 = 0.48$ and 0.55 with \overline{EVI}_{1km} and $EVI_{\varphi80}$, respectively, $p < 0.01$; Fig. 7). At a seasonal time scale, the correlations were still high for the greenup and senescence stages ($R_{adj}^2 = 0.45$ – 0.61 , $p < 0.01$), but substantially weakened during the maturity stage ($R_{adj}^2 = 0.01$, $p > 0.1$; $R_{adj}^2 = 0.16$, $p < 0.01$). Instead, for most of the meteorological classes, the variation in the daytime NEE during the maturity stage was more accounted for by the variation in the footprint-weighted land cover proportions ($P_{\varphi80}$; Fig. 8b). The R_{adj}^2 values from the multiple linear regression with $P_{\varphi80}$ were higher than the R_{adj}^2 values from the OLS regression with $EVI_{\varphi80}$ for a higher number of meteorological classes than the number of classes with the opposite R_{adj}^2 values. On the other hand, the daytime NEE during the greenup and senescence stages was poorly correlated with the $P_{\varphi80}$ ($R_{adj}^2 < 0.4$), and rather strongly driven by $EVI_{\varphi80}$ (R_{adj}^2 up to 0.7) for some meteorological classes. The nighttime NEE was not well correlated with either the $P_{\varphi80}$ or the $EVI_{\varphi80}$ ($R_{adj}^2 < 0.4$) regardless of phenological stage for most of the meteorological classes (Fig. 8d–f). The $P_{\varphi80}$ of DBF was the significant factor for most conditions (median p -value of all classes < 0.01 ; Fig. S10a), except for the greenup daytime (median p -value of all classes = 0.06), even when the correlation was weak. The $P_{\varphi80}$ of the other land covers, on the other hand, was mostly non-significant. During the daytime, the coefficient of $P_{\varphi80}$ of DBF was more negative than that of ENF during the maturity and senescence stages, less negative during the greenup stage (Fig. 9). During the nighttime, it was more positive than that of ENF regardless of the phenological stage (Fig. 9).

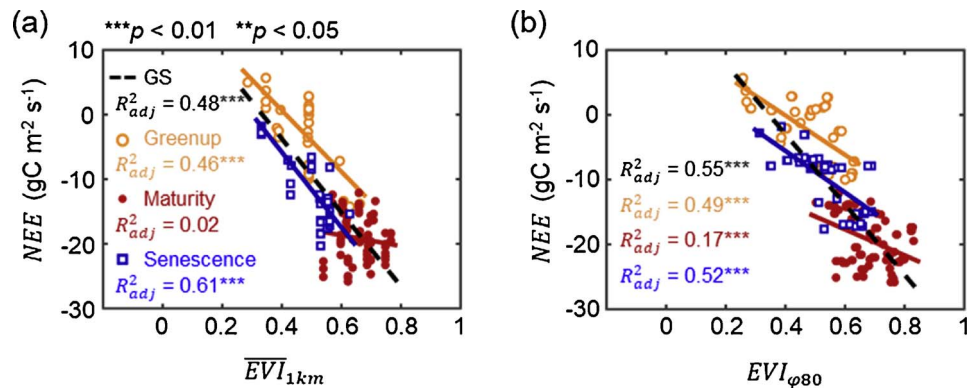


Fig. 7. The ordinary least squares (OLS) regressions between NEE and (a) the 1-km grid cell mean EVI (\overline{EVI}_{1km}), and (b) the footprint-weighted EVI ($EVI_{\varphi80}$) during entire growing season (GS), and during greenup, maturity and senescence stages for a meteorological condition (temperature, VPD, and PAR beyond the 75th percentile value of its cumulative distribution function; Fig. S4).

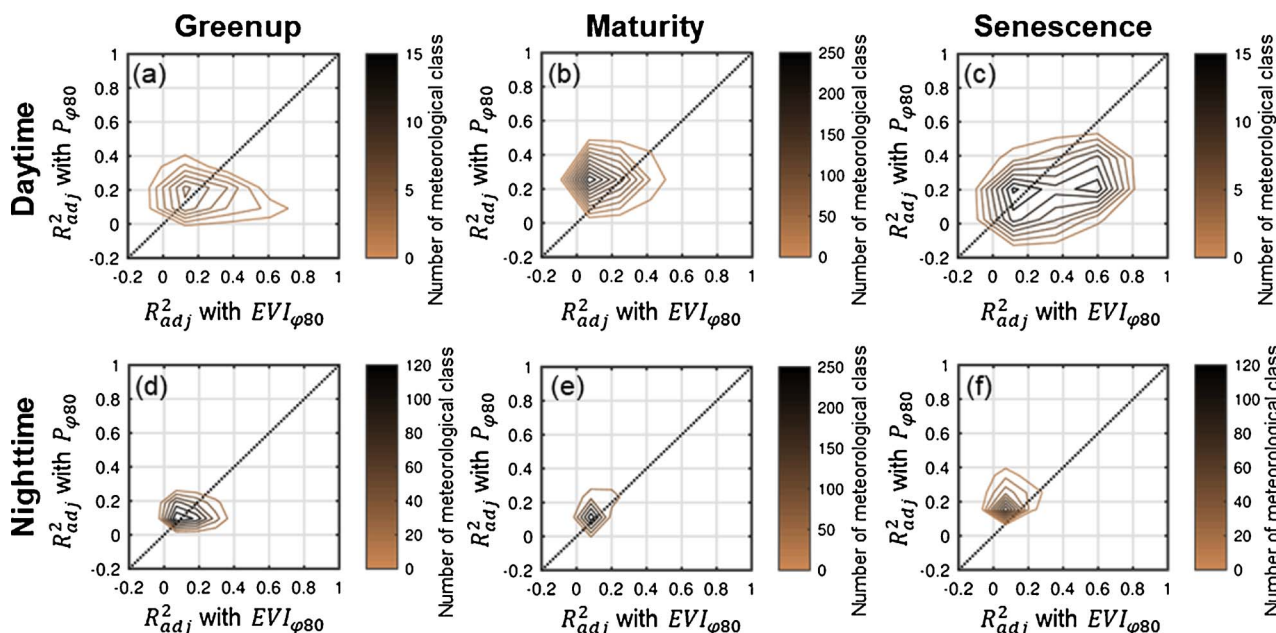


Fig. 8. Comparison of the adjusted coefficient of determination (R^2_{adj}) from the ordinary least square regression between NEE and footprint-weighted EVI ($EVI_{\phi80}$ in Eq. (3)) versus the R^2_{adj} from the multiple linear regression between NEE and footprint-weighted land cover proportions ($P_{\phi80}$; Eq. (4)) for the same meteorological class. The number of meteorological class having the R^2_{adj} values is shown in colored contours for each phenological stage (greenup on the first column, maturity on the second column, and senescence on the last column) during the daytime (a–c; $PAR > 50 \mu\text{mol m}^{-2} \text{s}^{-1}$) and nighttime (d–f), respectively.

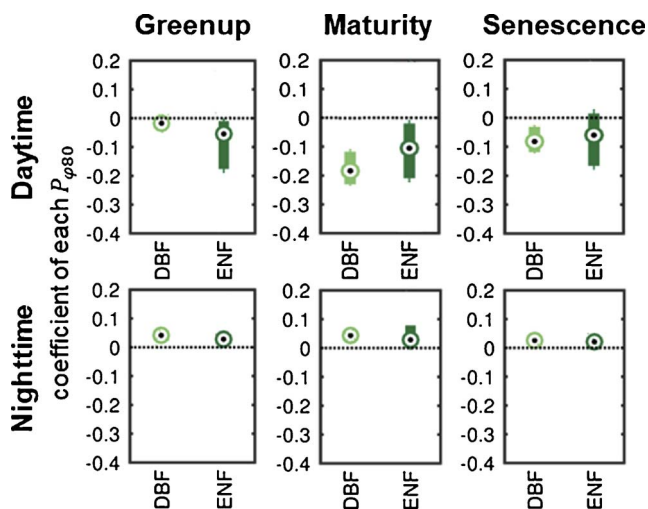


Fig. 9. The coefficients (i.e. NEE rate per unit land cover proportion ($\text{g C m}^{-2} \text{s}^{-1} \%^{-1}$)) of the two most dominant land covers (deciduous broadleaf forest (DBF) and evergreen needleleaf forest (ENF)) in the multiple linear regression between NEE and footprint-weighted land cover ($P_{\phi80}$) (Eq. (8)). The coefficients of the non-dominant land covers (mixed forest and woody wetland; each $P_{\phi80} < 5\%$) are presented in Fig. S10b. The regression was applied on each meteorological class for each phenological stage (greenup, maturity, and senescence) during the daytime (photosynthetically active radiation, $PAR > 50 \mu\text{mol m}^{-2} \text{s}^{-1}$) and nighttime, respectively. The box shows upper and lower quartile range of the coefficients from all meteorological classes and the black dots represent the median values.

4. Discussion

The study tower is located in a mixed forest where the landscape has gradually changed over the last decades, most noticeably with the expansion of two wetlands on the northwest and southeast sides from the tower (Fig. S7). Our principal goal in this study was to examine the spatial heterogeneity of the two surrounding spatial grid cells (1-km and 1.5-km) and the representativeness of the flux source area in capturing the vegetation characteristics (density magnitude and variation)

of the two surrounding grid cells during the daytime and nighttime, respectively, during each phenological stage (greenup, maturity, and senescence). As expected, the study site was mostly homogeneous during the maturity stage in the early 1990s, as the deciduous trees had fully developed to a closed canopy (Lévesque and King, 1999). The expansion of two woody wetlands then began to impact the closed canopy, increasing spatial heterogeneity within the 1-km grid cell, resulting in with up to 3.5 times higher *sill* values than those associated with the canopy in the early 1990s (Fig. 5b). However, their proportion in the flux source areas were still less than 5%. This explains why the flux measurements (i.e., NEE) were not very sensitive to this variability (median *p*-value of all classes > 0.05 ; Fig. S10). The impact of the changing landscape was also very dependent on its spatial scale. The landscape within the 1.5-km grid cell was already highly heterogeneous in the 1990s, so there was a less of a noticeable change in the seasonal patterns of the *sill* values over the study period (Fig. 5b). Daytime flux source weights mostly peaked along the southwest side around the tower and did not exceed the 1-km grid cell, while the nighttime flux source areas covered larger areas (Fig. 3). Both daytime and nighttime flux source areas were dominated by DBF regardless of the phenological stage, but the proportion of DBF during the nighttime was smaller and more variable than the proportion during the daytime (Fig. 4). Our results suggest that the daytime flux source areas cover a large enough area to adequately represent the vegetation density characteristics (distributions and magnitudes; Figs. 5c and 6, respectively) within the 1-km grid cell, but not those within the 1.5-km grid cell because of the additional non-vegetated land cover types at the northeastern corner of the grid cell (Fig. 1b). The vegetation density measures (\overline{EVI}_{1km} and $EVI_{\phi80}$), therefore, were well correlated with the daytime NEE except during the maturity stage (Figs. 7 and 8a–c). During the maturity stage, on the other hand, the variations in the footprint-weighted land cover proportions ($P_{\phi80}$) accounted for higher proportions of the variations in the daytime NEE for most meteorological classes (Fig. 8b). Meanwhile, the nighttime NEE had little correlation with either vegetation density ($EVI_{\phi80}$) or the land cover ($P_{\phi80}$) regardless of the phenological stages (Fig. 8d–f), perhaps suggesting that these factors do not account for much of the variation in soil respiration, which is the dominant

component of nighttime ecosystem respiration.

4.1. Study site spatial characteristics and flux source area representativeness

The *nugget effect* values of the 1-km grid cell reached almost zero during the entire growing season (Fig. 5a), which indicates that the sampling interval (i.e. 30 m of Landsat spatial resolution in this study) is appropriate to resolve the sources of spatial variation within the grid cell. Therefore, the Landsat data used in this study was suitable to assess the spatial representativeness of daytime flux source areas within the 1-km grid cell (Fig. 3). Nighttime flux source areas, however, often extended over a larger area under stable atmospheric conditions (Hadley and Schedlbauer, 2002; Kljun et al., 2002), therefore the 1.5-km surrounding area may be more applicable for the calibration and evaluation of lower resolution remote sensing-based estimates. However, the increased *nugget effect* values of the 1.5-km grid cell during the maturity and senescence stages (almost 10% of the *sill* values) indicate that the spatial representativeness of the 1.5-km grid cell needs to be assessed using a higher-spatial resolution data (e.g., higher resolution satellite imagery or aerial photographs) that are able to resolve the finer scale surface structures.

The *range* value can be considered to represent the effective size of the heterogeneity attributes (Kim et al., 2006). When a source area size (i.e., in this study, the geometric mean of along-wind and crosswind distances) is larger than the *range* value of the study grid cell, it can be assumed that the source area was large enough to represent the vegetation density variation in the study grid cell, and therefore, the source area is spatially-representative of the study grid cell (Kim et al., 2006). Over the study period, the *range* values of the 1-km grid cell were mostly less than or very close to the daytime source area extent throughout the entire growing season, and consistently smaller than the nighttime source area extent (Fig. 5c). This suggests that both the daytime and nighttime NEE measurements sufficiently reflect the variations in the vegetation density within the 1-km grid cell. The same interpretation can be applied for the 1.5-km grid cell during the daytime, but not during the nighttime when the *range* values mostly exceeded the source area extent.

The window size analysis generally corresponds with the semi-variogram results. The vegetation density around the tower is more heterogeneous than the density of the 1-km grid cell during the maturity stage, and smallest during the greenup stage (Fig. 6). The ΔEVI values are less than 5% of the 1-km average magnitudes within the source area during both the daytime and nighttime. This indicates that the source areas are generally large enough to represent the magnitude of the vegetation density within the 1-km grid cell during both the daytime and nighttime.

4.2. Significance of footprint-weighted land cover proportion

As stated, the source areas were spatially representative of both vegetation density variations and magnitudes within the 1-km grid cell during both the daytime and nighttime across all phenological stages. Therefore, the 1-km grid cell mean EVI (\overline{EVI}_{1km}), as well as MODIS 1-km EVI (Rahman et al., 2005; Tang et al., 2011; Xiao et al., 2004), can adequately account for the variation in the daytime NEE as much as the footprint-weighted EVI ($EVI_{\varphi 80}$) can (Fig. 7). Specifically, the high correlations between the vegetation density measures (\overline{EVI}_{1km} and $EVI_{\varphi 80}$) and the daytime NEE were primarily driven by the phenological development of the deciduous trees during the entire growing season and particularly during the greenup and senescence stages (EVI rises/drops by about 0.4). Therefore, the land cover variations within the source area had little effect on the daytime NEE during those periods. However, both \overline{EVI}_{1km} and $EVI_{\varphi 80}$ can hardly account for the variation in the daytime NEE during the maturity stage, when both DBF and ENF have similar EVI values (Fig. 1c), and the vegetation carbon uptake

primarily depends on its physiological response to meteorological variables, such as solar radiation, temperature, and soil moisture (Gao et al., 2014; Jahan and Gan, 2009; Tang et al., 2012). Yet, however, the mean response functions of a single vegetation functional type (DBF) accounted for only about 50% of the interannual variations in the NEE at the study site (Urbanski et al., 2007). Our results may provide a better explanation of the variation in the daytime NEE especially during foliage maturity (Fig. 8b). It was expected that the $P_{\varphi 80}$ of DBF is the most significant factor in the flux measurements at the study tower, given the dominance of DBF around the study tower (Urbanski et al., 2007), but it hadn't yet been quantitatively assessed for each phenological stage. The stronger contribution of the $P_{\varphi 80}$ of DBF (a more negative coefficient; Fig. 9) than that of ENF corresponds well to the higher carbon uptake rates of deciduous trees than the ones of coniferous trees during the maturity stage (Hadley et al., 2008). Although the $P_{\varphi 80}$ of ENF was not a significant factor on the daytime NEE across the phenological stages, the greater negative coefficient of the $P_{\varphi 80}$ of ENF (representing a stronger contribution) during the greenup stage than that of DBF reflects the higher carbon uptake rates of the ENF than the DBF at the study site at the beginning of the growing season (Hadley et al., 2008). The similar coefficient values of the $P_{\varphi 80}$ for both the DBF and ENF during the senescence stage (Fig. 9) may result from the strong regulation of other factors, such as day length (Bauerle et al., 2012) and soil moisture (Hwang et al., 2014; Urbanski et al., 2007), rather than by leaf presence at the end of growing season.

Meanwhile, although the variations in the source area during the nighttime were higher than those during the daytime, the nighttime NEE was only rather weakly correlated with either $EVI_{\varphi 80}$ or $P_{\varphi 80}$ across all phenological stages. This could be largely attributed to the similar rates of soil respiration at both DBF and ENF at the study site (Giasson et al., 2013).

Note that the significances and sensitivities of the measured NEE to the footprint-weighted land cover proportions ($P_{\varphi 80}$; Eq. (4)) are subject to uncertainties in the NLCD products and also to the limited NLCD availability (only 3 products over the 13 years study period).

4.3. Implication for gap-filling process and upscaling strategies

To date the most common practice for filling gaps in hourly NEE measurements is to derive estimates from mean temperature- and light-response functions (Falge et al., 2001). Uncertainty is therefore introduced because those response functions are not intended to respond to the short-time variations in the meteorological drivers, but to characterize the ecosystem-scale mean response for a certain time period (in days or weeks) (Falge et al., 2001; Stoy et al., 2006). The isotopic eddy covariance flux data also showed that the ecosystem respiration values at the study tower were dependent on the wind direction, therefore the source area variations (Wehr and Saleska, 2015). Our result indicates the dependence of the daytime NEE on the footprint-weighted land cover variations during the maturity stage, and addresses potential biases resulting from a discrepancy between the spatiotemporally-integrated mean ecosystem and the hourly-varying flux source areas. Therefore, this could cause misinterpretations of ecosystem short-term sensitivity to climate change and to the biome characteristics across multiple sites. In practice, it remains difficult to separate the flux measurements by upwind land cover types because it introduces additional uncertainties as the number of points in each bin available for calibration is substantially reduced. However, our analyses highlight the importance of considering the unique site-specific landscape conditions in the gap-filling process, especially during the peak growing season (i.e. the maturity stage) (Falge et al., 2001; Moffat et al., 2007).

Previous studies have investigated the implication of the source area variation on upwind vegetation density and meteorological factors when upscaling the measured flux to regional scales (Fu et al., 2014; Xu et al., 2017). However, vegetation dynamics (such as photosynthesis and respiration) do not necessarily respond linearly to these individual

drivers (Urbanski et al., 2007), especially in water-limited ecosystems (Novick et al., 2015), and in dense canopies during the peak growing season when the canopy is fully developed (Fig. 7; Urbanski et al., 2007). The vegetation response to these drivers also varies greatly between the vegetation types (Daley et al., 2007; Hadley et al., 2008). Therefore, in the process of calibrating the upscaling coefficients using flux measurements, the source weight should be applied to the vegetation response (i.e. the flux) depending on its type, rather than on its individual flux source attributes (i.e. vegetation density or meteorological factors). The coefficient of the multiple linear regression, i.e., the NEE rate per unit land cover proportion ($\text{g C m}^{-2} \text{s}^{-1} \%^{-1}$) for the given meteorological class, can be up-scaled using the proportions of the significant land covers within the grid cell of interest (e.g. 1-km).

5. Conclusion

We assessed the long-term spatial heterogeneity around the study flux tower using remote sensing datasets, and examined the representativeness of the flux measurements for the surrounding area (1-km and 1.5-km grid cells, respectively) during the daytime and nighttime, respectively, during each phenological stage (greenup, maturity, and senescence). In our study site, the forested landscape had gradually shifted since 2001, resulting in an increase in spatial heterogeneity within the 1-km grid cell centered at the flux tower, especially during the maturity stage. Yet, the daytime flux source area remained spatially representative for vegetation characteristics (both density and type) within this 1-km grid cell over the course of various landscape transitions. We have demonstrated that the relevant flux source attribute, governing more variation in the NEE, differed between phenological stages. The variation in the daytime NEE is highly correlated with the vegetation density (EVI in this study) during the phenological transition stages (greenup and senescence), but the variation during the maturity stage was better captured by the footprint-weighted land cover proportion. The nighttime NEE was hardly affected by the variation in either the vegetation density or the land cover proportion.

Our study highlights the importance of accounting for variation in the footprint-weighted land cover in mixed-land cover regions (1) for interpretation of variations in flux measurements, (2) to fill data gaps, and (3) to upscale the flux measurements to larger scales. In this study, we only analyzed flux measurements from a single tower site (the tower that provides the longest flux record in the US) as a case study. Our approach can be further applied to other existing tower sites as there are increasing numbers of flux towers with multi-decadal flux measurements. Our results suggest a consideration of the land cover variations contributing to the measured flux will result in a better understanding of ecosystem response to environmental forcing in a changing climate.

Acknowledgements

The authors are grateful for the two anonymous reviewers whose comments have greatly improved the manuscript. We appreciate the efforts of Taejin Park in providing the processed LVIS data. We also would like to thank Dr. Miguel O. Roman for sharing the detailed methodology of semi-variogram analysis using Landsat data and Dr. Kimberly Novick for constructive comments on an earlier version of the manuscript. This study was financially supported in part by the NASA MODIS science team (Grant No. NNX11AD58G), the NASA Carbon Science program (Grant No. NNX17AE69G), and the USGS Science Team (Grant No. ING12PC00072). The Harvard Forest EMS flux tower has been supported by the Office of Science (BER) at the US Department of Energy (DOE) under various sub-programs over the years, and it is now a core site in AmeriFlux network (Grant No. DE-AC02-05CH11231). The long-term meteorological and hydrological measurements at Harvard Forest are also supported through the National Science Foundation Long-Term Ecological Research Programs (Grant

No. NSF-DEB-1237491). The Harvard Forest LTER data were obtained from the archive at (<http://harvardforest.fas.harvard.edu/harvard-forest-data-archive>).

Appendix A. Supplementary data

Supplementary material related to this article can be found, in the online version, at doi:<https://doi.org/10.1016/j.agrformet.2018.02.004>.

References

- Amiro, B.D., 1998. Footprint climatologies for evapotranspiration in a boreal catchment. *Agric. For. Meteorol.* 90, 195–201. [http://dx.doi.org/10.1016/S0168-1923\(97\)00096-8](http://dx.doi.org/10.1016/S0168-1923(97)00096-8).
- Baldocchi, D.D., 2003. Assessing the eddy covariance technique for evaluating carbon dioxide exchange rates of ecosystems: past, present and future. *Global Change Biol.* 9, 479–492. <http://dx.doi.org/10.1046/j.1365-2486.2003.00629.x>.
- Baldocchi, D.D., Hincks, B.B., Meyers, T.P., 1988. Measuring biosphere-atmosphere exchanges of biologically related gases with micrometeorological methods. *Ecology* 69, 1331. <http://dx.doi.org/10.2307/1941631>.
- Battles, J.J., Robards, T., Das, A., Waring, K., Gilles, J.K., Biging, G., Schurr, F., 2007. Climate change impacts on forest growth and tree mortality: a data-driven modeling study in the mixedconifer forest of the Sierra Nevada, California. *Clim. Change* 87. <http://dx.doi.org/10.1007/s10584-007-9358-9>.
- Bauerle, W.L., Oren, R., Way, D.A., Qian, S.S., Stoy, P.C., Thornton, P.E., Bowden, J.D., Hoffman, F.M., Reynolds, R.F., 2012. Photoperiodic regulation of the seasonal pattern of photosynthetic capacity and the implications for carbon cycling. *Proc. Natl. Acad. Sci. U. S. A.* 109, 8612–8617. <http://dx.doi.org/10.1073/pnas.1119131109>.
- Belmecheri, S., Maxwell, R.S., Taylor, A.H., Davis, K.J., Freeman, K.H., Munger, J.W., 2014. Tree-ring $\delta^{13}\text{C}$ tracks flux tower ecosystem productivity estimates in a NE temperate forest. *Environ. Res. Lett.* 9, 74011. <http://dx.doi.org/10.1088/1748-9326/9/7/074011>.
- Cao, M., Woodward, F.I., 1998. Dynamic responses of terrestrial ecosystem carbon cycling to global climate change. *Nature* 393, 249–252. <http://dx.doi.org/10.1038/30460>.
- Carroll, S.S., Cressie, N., 1996. A comparison of geostatistical methodologies used to estimate snow water equivalent. *J. Am. Water Resour. Assoc.* 32, 267–278. <http://dx.doi.org/10.1111/j.1752-1688.1996.tb03450.x>.
- Chasmer, L., Kljun, N., Hopkinson, C., Brown, S., Milne, B.T., Giroux, K., Barr, A.G., Devito, K.J., Creed, I.F., Petrone, R., 2011. Characterizing vegetation structural and topographic characteristics sampled by eddy covariance within two mature aspen stands using lidar and a flux footprint model: scaling to MODIS. *J. Geophys. Res. Biogeosci.* 116, 1–19. <http://dx.doi.org/10.1029/2010JG001567>.
- Chen, B., Coops, N.C., Fu, D., Margolis, H.A., Amiro, B.D., Black, T.A., Arain, M.A., Barr, A.G., Bourque, C.P.-A., Flanagan, L.B., Lafleur, P.M., McCaughey, H., Wofsy, S.C., 2012. Characterizing spatial representativeness of flux tower eddy-covariance measurements across the Canadian carbon program network using remote sensing and footprint analysis. *Remote Sens. Environ.* 124, 742–755. <http://dx.doi.org/10.1016/j.rse.2012.06.007>.
- Chen, B., Zhang, H., Coops, N.C., Fu, D., Worthy, D.E.J., Xu, G., Black, T.A., 2013. Assessing scalar concentration footprint climatology and land surface impacts on tall-tower CO₂ concentration measurements in the boreal forest of central Saskatchewan, Canada. *Theor. Appl. Climatol.* 118, 115–132. <http://dx.doi.org/10.1007/s00704-013-1038-2>.
- Curran, P., 1988. The semi-variogram in remote sensing: an introduction. *Remote Sens. Environ.* 507, 493–507. [http://dx.doi.org/10.1016/0034-4257\(88\)90021-1](http://dx.doi.org/10.1016/0034-4257(88)90021-1).
- Daley, M.J., Phillips, N.G., Pettijohn, C., Hadley, J.L., 2007. Water use by eastern hemlock (*Tsuga canadensis*) and black birch (*Betula lenta*): implications of effects of the hemlock woolly adelgid. *Can. J. For. Res.* 37, 2031–2040. <http://dx.doi.org/10.1139/X07-045>.
- Davidson, E.A., Richardson, A.D., Savage, K.E., Hollinger, D.Y., 2006. A distinct seasonal pattern of the ratio of soil respiration to total ecosystem respiration in a spruce-dominated forest. *Global Change Biol.* 12, 230–239. <http://dx.doi.org/10.1111/j.1365-2486.2005.01062.x>.
- Davis, J.C., 1986. *Statistics and Data Analysis in Geology*, vol. 1 Wiley.
- Falge, E.M., Baldocchi, D.D., Olson, R., Anthoni, P., Aubinet, M., Bernhofer, C., Burba, G., Ceulemans, R., Clement, R., Dolman, H., Granier, A., Gross, P., Grünwald, T., Hollinger, D.Y., Jensen, N.-O., Katul, G.G., Keronen, P., Kowalski, A.S., Lai, C.T., Law, B.E., Meyers, T.P., Moncrieff, J., Moors, E., Munger, J.W., Pilegaard, K., Rannik, Ü., Rebmann, C., Suyker, A., Tenhunen, J., Tu, K., Verma, S.B., Vesala, T., Wilson, K.B., Wofsy, S.C., 2001. Gap filling strategies for defensible annual sums of net ecosystem exchange. *Agric. For. Meteorol.* 107, 43–69. [http://dx.doi.org/10.1016/S0168-1923\(00\)00225-2](http://dx.doi.org/10.1016/S0168-1923(00)00225-2).
- Falge, E.M., Baldocchi, D.D., Tenhunen, J., Aubinet, M., Bakwin, P., Berbigier, P., Bernhofer, C., Burba, G., Clement, R., Davis, K.J., Elbers, J.A., Goldstein, A.H., Grelle, A., Granier, A., Guðmundsson, J., Hollinger, D.Y., Kowalski, A.S., Katul, G.G., Law, B.E., Malhi, Y., Meyers, T.P., Monson, R.K., Munger, J.W., Oechel, W.C., Paw, U., Pilegaard, K., Rannik, U., Rebmann, C., Suyker, A., Valentini, R., Wilson, K., Wofsy, S., 2002. Seasonality of ecosystem respiration and gross primary production as derived from FLUXNET measurements. *Agric. For. Meteorol.* 113, 53–74. [http://dx.doi.org/10.1016/S0168-1923\(02\)00102-8](http://dx.doi.org/10.1016/S0168-1923(02)00102-8).
- Finzi, A.C., Austin, A.T., Cleland, E.E., Frey, S.D., Houlton, B.Z., Wallenstein, M.D., 2011.

- Responses and feedbacks of coupled biogeochemical cycles to climate change: examples from terrestrial ecosystems. *Front. Ecol. Environ.* 9, 61–67. <http://dx.doi.org/10.1890/100001>.
- Fu, D., Chen, B., Zhang, H., Wang, J., Black, T.A., Amiro, B.D., Bohrer, G., Bolstad, P.V., Coulter, R., Rahman, A.F., Dunn, A.L., McCaughey, H., Meyers, T.P., Verma, S.B., 2014. Estimating landscape net ecosystem exchange at high spatial–temporal resolution based on landsat data, an improved upscaling model framework, and eddy covariance flux measurements. *Remote Sens. Environ.* 141, 90–104. <http://dx.doi.org/10.1016/j.rse.2013.10.029>.
- Gao, X., 2000. Optical–Biophysical relationships of vegetation spectra without background contamination. *Remote Sens. Environ.* 74, 609–620. [http://dx.doi.org/10.1016/S0034-4257\(00\)00150-4](http://dx.doi.org/10.1016/S0034-4257(00)00150-4).
- Gao, Y., Yu, G., Yan, H., Zhu, X., Li, S., Wang, Q., Zhang, J., Wang, Y., Li, Y., Zhao, L., Shi, P., 2014. A MODIS-based photosynthetic capacity model to estimate gross primary production in Northern China and the Tibetan Plateau. *Remote Sens. Environ.* 148, 108–118. <http://dx.doi.org/10.1016/j.rse.2014.03.006>.
- Giasson, M.-A., Ellison, A.M., Bowden, R.D., Crill, P.M., Davidson, E.A., Drake, J.E., Frey, S.D., Hadley, J.L., Lavine, M., Melillo, J.M., Munger, J.W., Nadelhoffer, K.J., Nicoll, L., Ollinger, S.V., Savage, K.E., Steudler, P.A., Tang, J., Varner, R.K., Wofsy, S.C., Foster, D.R., Finzi, A.C., 2013. Soil respiration in a northeastern US temperate forest: a 22-year synthesis. *Ecosphere* 4, art140. <http://dx.doi.org/10.1890/ES13.00183.1>.
- Göckede, M., Foken, T., Aubinet, M., Aurela, M., Banja, J., Bernhofer, C., Bonnefond, J.M., Brunet, Y., Carrara, A., Clement, R., Dellwik, E., Elbers, J., Eugster, W., Führer, J., Granier, A., Grünwald, T., Heinesch, B., Janssens, I.A., Knohl, A., Koeble, R., Laurila, T., Longdoz, B., Manca, G., Marek, M., Markkanen, T., Mateus, J., Matteucci, G., Mauder, M., Migliavacca, M., Minerbi, S., Moncrieff, J., Montagnani, L., Moors, E., Ourcival, J.-M., Papale, D., Pereira, J., Pilegaard, K., Pita, G., Rambal, S., Rebmann, C., Rodrigues, A., Rotenberg, E., Sanz, M., Sedlak, P., Seufert, G., Siebicke, L., Soussana, J.F., Valentini, R., Vesala, T., Verbeeck, H., Yakir, D., 2008. Quality control of CarboEurope flux data – part 1: coupling footprint analyses with flux data quality assessment to evaluate sites in forest ecosystems. *Biogeosciences* 5, 433–450. <http://dx.doi.org/10.5194/bg-5-433-2008>.
- Goulden, M.L., Munger, J.W., Fan, S.-M., Daube, B.C., Wofsy, S.C., 1996. Measurements of carbon sequestration by long-term eddy covariance: methods and a critical evaluation of accuracy. *Global Change Biol.* 2, 169–182. <http://dx.doi.org/10.1111/j.1365-2486.1996.tb00070.x>.
- Griebel, A., Bennett, L.T., Metzger, D., Cleverly, J., Burba, G., Arndt, S.K., 2016. Effects of inhomogeneities within the flux footprint on the interpretation of seasonal, annual, and interannual ecosystem carbon exchange. *Agric. For. Meteorol.* 221, 50–60. <http://dx.doi.org/10.1016/j.agrformet.2016.02.002>.
- Hadley, J.L., Kuzeja, P.S., Daley, M.J., Phillips, N.G., Mulcahy, T., Singh, S., 2008. Water use and carbon exchange of red oak- and eastern hemlock-dominated forests in the northeastern USA: implications for ecosystem-level effects of hemlock woolly adelgid. *Tree Physiol.* 28, 615–627. <http://dx.doi.org/10.1093/treephys/28.4.615>.
- Hadley, J.L., Schedlbauer, J.L., 2002. Carbon exchange of an old-growth eastern hemlock (*Tsuga canadensis*) forest in central New England. *Tree Physiol.* 22, 1079–1092. <http://dx.doi.org/10.1093/treephys/22.15-16.1079>.
- Haylock, M.R., Hofstra, N., Klein Tank, A.M.G., Klok, E.J., Jones, P.D., New, M., 2008. A European daily high-resolution gridded data set of surface temperature and precipitation for 1950–2006. *J. Geophys. Res. Atmos.* 113. <http://dx.doi.org/10.1029/2008JD010201>.
- Heinsch, F.A., Zhao, Maosheng, Running, S.W., Kimball, J.S., Nemani, R.R., Davis, K.J., Bolstad, P.V., Cook, B.D., Desai, A.R., Ricciuto, D.M., Law, B.E., Oechel, W.C., Kwon, Hoyjung, Luo, Hongyan, Wofsy, S.C., Dunn, A.L., Munger, J.W., Baldocchi, D.D., Xu, Liukang, Hollinger, D.Y., Richardson, A.D., Stoy, P.C., Siqueira, M.B.S., Monson, R.K., Burns, S.P., Flanagan, L.B., 2006. Evaluation of remote sensing based terrestrial productivity from MODIS using regional tower eddy flux network observations. *IEEE Trans. Geosci. Remote Sens.* 44, 1908–1925. <http://dx.doi.org/10.1109/TGRS.2005.853936>.
- Hsieh, C., Katul, G., Chi, T., 2000. An approximate analytical model for footprint estimation of scalar fluxes in thermally stratified atmospheric flows. *Adv. Water Resour.* 23, 765–772. [http://dx.doi.org/10.1016/S0309-1708\(99\)00042-1](http://dx.doi.org/10.1016/S0309-1708(99)00042-1).
- Huete, A.R., Didan, K., Miura, T., Rodriguez, E., Gao, X., Ferreira, L., 2002. Overview of the radiometric and biophysical performance of the MODIS vegetation indices. *Remote Sens. Environ.* 83, 195–213. [http://dx.doi.org/10.1016/S0034-4257\(02\)00096-2](http://dx.doi.org/10.1016/S0034-4257(02)00096-2).
- Hutjes, R.W.A., Vellinga, O.S., Gioli, B., Miglietta, F., 2010. Dis-aggregation of airborne flux measurements using footprint analysis. *Agric. For. Meteorol.* 150, 966–983. <http://dx.doi.org/10.1016/j.agrformet.2010.03.004>.
- Hwang, T., Band, L.E., Miniati, C.F., Song, C., Bolstad, P.V., Vose, J.M., Love, J.P., 2014. Divergent phenological response to hydroclimate variability in forested mountain watersheds. *Global Change Biol.* 20, 2580–2595. <http://dx.doi.org/10.1111/gcb.12556>.
- Hwang, T., Song, C., Vose, J.M., Band, L.E., 2011. Topography-mediated controls on local vegetation phenology estimated from MODIS vegetation index. *Lands. Ecol.* 26, 541–556. <http://dx.doi.org/10.1007/s10980-011-9580-8>.
- Jahan, N., Gan, T.Y., 2009. Modeling gross primary production of deciduous forest using remotely sensed radiation and ecosystem variables. *J. Geophys. Res.* 114, G04026. <http://dx.doi.org/10.1029/2008JG000919>.
- Keenan, T.F., Gray, J., Friedl, M.A., Toomey, M., Bohrer, G., Hollinger, D.Y., Munger, J.W., O’Keefe, J., Schmid, H.P., Wing, I.S., Yang, B., Richardson, A.D., 2014. Net carbon uptake has increased through warming-induced changes in temperate forest phenology. *Nat. Clim. Change* 4, 598–604. <http://dx.doi.org/10.1038/nclimate2253>.
- Keenan, T.F., Hollinger, D.Y., Bohrer, G., Dragoni, D., Munger, J.W., Schmid, H.P., Richardson, A.D., 2013. Increase in forest water-use efficiency as atmospheric carbon dioxide concentrations rise. *Nature* 499, 324–327. <http://dx.doi.org/10.1038/nature12291>.
- Kim, J., Guo, Q., Baldocchi, D.D., Leclerc, M., Xu, L., Schmid, H.P., 2006. Upscaling fluxes from tower to landscape: overlaying flux footprints on high-resolution (IKONOS) images of vegetation cover. *Agric. For. Meteorol.* 136, 132–146. <http://dx.doi.org/10.1016/j.agrformet.2004.11.015>.
- Kim, J., Hwang, T., Schaaf, C.L., Orwig, D.A., Boose, E., Munger, J.W., 2017. Increased water yield due to the hemlock woolly adelgid infestation in New England. *Geophys. Res. Lett.* 2327–2335. <http://dx.doi.org/10.1002/2016GL072327>.
- Kljun, N., Calanca, P., Rotach, M.W., Schmid, H.P., 2015. A simple two-dimensional parameterisation for Flux Footprint Prediction (FFP). *Geosci. Model Dev.* 8, 3695–3713. <http://dx.doi.org/10.5194/gmd-8-3695-2015>.
- Kljun, N., Calanca, P., Rotach, M.W., Schmid, H.P., 2004. A simple parameterisation for flux footprint predictions. *Bound.-Layer Meteorol.* 112, 503–523. <http://dx.doi.org/10.1023/B:BOUN.0000030653.71031.96>.
- Kljun, N., Rotach, M.W., Schmid, H.P., 2002. A three-dimensional backward lagrangian footprint model for a wide range of boundary-layer stratifications. *Bound.-Layer Meteorol.* 103, 205–226. <http://dx.doi.org/10.1023/A:1014556300021>.
- Kormann, R., Meixner, F.X., 2001. An analytical footprint model for non-neutral stratification. *Bound.-Layer Meteorol.* 99, 207–224. <http://dx.doi.org/10.1023/A:1018991015119>.
- Law, B., Falge, E.M., Gu, L., Baldocchi, D.D., Bakwin, P., Berbigier, P., Davis, K., Dolman, A., Falk, M., Fuentes, J., Goldstein, A., Granier, A., Grelle, A., Hollinger, D., Janssens, I., Jarvis, P., Jensen, N., Katul, G., Mahli, Y., Matteucci, G., Meyers, T., Monson, R., Munger, J.W., Oechel, W.C., Olson, R., Pilegaard, K., Paw Uh, K.T., Thorgeirsson, H., Valentini, R., Verma, S., Vesala, T., Wilson, K., Wofsy, S., 2002. Environmental controls over carbon dioxide and water vapor exchange of terrestrial vegetation. *Agric. For. Meteorol.* 113, 97–120. [http://dx.doi.org/10.1016/S0168-1923\(02\)00104-1](http://dx.doi.org/10.1016/S0168-1923(02)00104-1).
- Lévesque, J., King, D.J., 1999. Airborne digital camera image semivariance for evaluation of forest structural damage at an acid mine site. *Remote Sens. Environ.* 68, 112–124. [http://dx.doi.org/10.1016/S0034-4257\(98\)00104-7](http://dx.doi.org/10.1016/S0034-4257(98)00104-7).
- Masek, J.G., Vermote, E.F., Saleous, N.E., Wolfe, R.E., Hall, F.G., Huemmrich, K.F., Gao, F., Kutler, J., Lim, T., 2006. A landsat surface reflectance dataset. *IEEE Geosci. Remote Sens. Lett.* 3, 68–72. <http://dx.doi.org/10.1109/LGRS.2005.857030>.
- Matheron, G., 1963. Principles of geostatistics. *Econ. Geol.* 58, 1246–1266. <http://dx.doi.org/10.2113/gsecongeo.58.8.1246>.
- Menzer, O., Pastorello, G., Metzger, S., Poindexter, C., Agarwal, D., Papale, D., 2014. Mapping AmeriFlux footprints: towards knowing the flux source area across a network of towers. *American Geophysical Union, Fall Meeting 2014. Abstract #B53A-0155*.
- Menzer, O., Pastorello, G., Metzger, S.R.L., Poindexter, C., Agarwal, D., Papale, D., 2015. Mapping AmeriFlux footprints: towards deconvolving spatial and temporal co-variation across a network of flux towers. *5th NACP All-Investigators Meeting*.
- Moffat, A.M., Papale, D., Reichstein, M., Hollinger, D.Y., Richardson, A.D., Barr, A.G., Beckstein, C., Braswell, B.H., Churkina, G., Desai, A.R., Falge, E.M., Gove, J.H., Heimann, M., Hui, D., Jarvis, A.J., Kattge, J., Noormets, A., Stauch, V.J., 2007. Comprehensive comparison of gap-filling techniques for eddy covariance net carbon fluxes. *Agric. For. Meteorol.* 147, 209–232. <http://dx.doi.org/10.1016/j.agrformet.2007.08.011>.
- Munger, J.W., Wofsy, S.C., 1999a. Biomass inventories at harvard forest EMS tower since 1993. *Environmental Data Initiative*. <http://dx.doi.org/10.6073/pasta/8c1c49009eda396ae7ad48e2f0dd4eca>. [WWW Document].
- Munger, J.W., Wofsy, S.C., 1999b. Canopy-atmosphere exchange of carbon, water and energy at harvard forest EMS tower since 1991. *Environmental Data Initiative*. <http://dx.doi.org/10.6073/pasta/1580a910a8a1a154cb59c941b252613a>. [WWW Document].
- Nemani, R.R., Keeling, C.D., Hashimoto, H., Jolly, W.M., Piper, S.C., Tucker, C.J., Myeni, R.B., Running, S.W., 2003. Climate-driven increases in global terrestrial net primary production from 1982 to 1999. *Science* 80 (300), 1560–1563. <http://dx.doi.org/10.1126/science.1082750>.
- Noréus, J.P., Nyberg, M.R., Hayling, K.L., 1997. The gravity anomaly field in the Gulf of Bothnia spatially characterized from satellite altimetry and in situ measurements. *J. Appl. Geophys.* 37, 67–84. [http://dx.doi.org/10.1016/S0926-9851\(97\)00007-4](http://dx.doi.org/10.1016/S0926-9851(97)00007-4).
- Novick, K.A., Brantley, S.T., Miniati, C.F., Walker, J., Vose, J.M., 2014. Inferring the contribution of advection to total ecosystem scalar fluxes over a tall forest in complex terrain. *Agric. For. Meteorol.* 185, 1–13. <http://dx.doi.org/10.1016/j.agrformet.2013.10.010>.
- Novick, K.A., Oishi, C.A., Ward, E.J., Siqueira, M.B.S., Juang, J.-Y., Stoy, P.C., Oishi, A.C., Ward, E.J., Siqueira, M.B.S., Juang, J.-Y., Stoy, P.C., 2015. On the difference in the net ecosystem exchange of CO₂ between deciduous and evergreen forests in the southeastern United States. *Glob. Change Biol.* 21, 827–842. <http://dx.doi.org/10.1111/gcb.12723>.
- O’Keefe, J., 2000. Phenology of woody species at Harvard forest since 1990. *Environmental Data Initiative*. <http://dx.doi.org/10.6073/pasta/bf1e4d2f198ab9b02da82154236b0816>. [WWW Document].
- Oishi, C.A., Oren, R., Stoy, P.C., 2008. Estimating components of forest evapotranspiration: A footprint approach for scaling sap flux measurements. *Agric. For. Meteorol.* 148, 1719–1732. <http://dx.doi.org/10.1016/j.agrformet.2008.06.013>.
- Orwig, D.A., Cobb, R.C., D’Amato, A.W., Kizilinski, M.L., Foster, D.R., 2008. Multi-year ecosystem response to hemlock woolly adelgid infestation in southern New England forests. *Can. J. For. Res.* 38, 834–843. <http://dx.doi.org/10.1139/X07-196>.
- Park, T., Kennedy, R., Choi, S., Wu, J., Lefsky, M., Bi, J., Mantooth, J., Myeni, R., Knazikhin, Y., 2014. Application of physically-based slope correction for maximum forest canopy height estimation using waveform lidar across different footprint sizes and locations: tests on LVIS and GLAS. *Remote Sens.* 6, 6566–6586. <http://dx.doi.org/10.3390/rs6076566>.

- Pastorello, G., Agarwal, D., Papale, D., Samak, T., Trotta, C., Ribeca, A., Poindexter, C., Faybishenko, B., Gunter, D., Hollowgrass, R., Canfora, E., 2014. Observational data patterns for time series data quality assessment. In: Proceedings of the 2014 IEEE 10th International Conference on E-Science - Volume 01, E-SCIENCE' 14. IEEE Computer Society, Washington, DC, USA. pp. 271–278. <http://dx.doi.org/10.1109/eScience.2014.45>.
- Phillips, S.C., Varner, R.K., Frohling, S., Munger, J.W., Bubier, J.L., Wofsy, S.C., Crill, P.M., 2010. Interannual, seasonal, and diel variation in soil respiration relative to ecosystem respiration at a wetland to upland slope at Harvard forest. *J. Geophys. Res.* 115, 1–18. <http://dx.doi.org/10.1029/2008JG000858>.
- Rahman, A.F., Sims, D.A., Cordova, V.D., El-Masri, B.Z., 2005. Potential of MODIS EVI and surface temperature for directly estimating per-pixel ecosystem C fluxes. *Geophys. Res. Lett.* 32, L19404. <http://dx.doi.org/10.1029/2005GL024127>.
- Román, M.O., Schaaf, C.L., Woodcock, C.E., Strahler, A.H., Yang, X., Braswell, B.H., Curtis, P.S., Davis, K.J., Dragoni, D., Goulden, M.L., 2009. The MODIS (Collection V005) BRDF/albedo product: assessment of spatial representativeness over forested landscapes. *Remote Sens. Environ.* 113, 2476–2498. <http://dx.doi.org/10.1016/j.rse.2009.07.009>.
- Savage, K.E., Davidson, E.A., 2001. Interannual variation of soil respiration in two New England forests. *Global Biogeochem. Cycles* 15, 337–350. <http://dx.doi.org/10.1029/1999GB001248>.
- Schmid, H.P., 1997. Experimental design for flux measurements: matching scales of observations and fluxes. *Agric. For. Meteorol.* 87, 179–200. [http://dx.doi.org/10.1016/S0168-1923\(97\)00011-7](http://dx.doi.org/10.1016/S0168-1923(97)00011-7).
- Schmid, H.P., 1994. Source areas for scalars and scalar fluxes. *Bound.-Layer Meteorol.* 67, 293–318. <http://dx.doi.org/10.1007/BF00713146>.
- Schmid, H.P., Grimmond, C.S.B., Cropley, F.D., Offerle, B., Su, H.-B., 2000. Measurements of CO₂ and energy fluxes over a mixed hardwood forest in the mid-western United States. *Agric. For. Meteorol.* 103, 357–374. [http://dx.doi.org/10.1016/S0168-1923\(00\)00140-4](http://dx.doi.org/10.1016/S0168-1923(00)00140-4).
- Schmid, H.P., Lloyd, C.R., 1999. Spatial representativeness and the location bias of flux footprints over inhomogeneous areas. *Agric. For. Meteorol.* 93, 195–209. [http://dx.doi.org/10.1016/S0168-1923\(98\)00119-1](http://dx.doi.org/10.1016/S0168-1923(98)00119-1).
- Schwalm, C.R., Williams, Ca., Schaefer, K., Anderson, R., Arain, M.A., Baker, I., Barr, A., Black, T.A., Chen, G., Chen, J.M., Ciais, P., Davis, K.J., Desai, A., Dietze, M., Dragoni, D., Fischer, M.L., Flanagan, L.B., Grant, R., Gu, L., Hollinger, D., Izaurralde, R.C., Kucharik, C.J., Lafleur, P., Law, B.E., Li, L., Li, Z., Liu, S., Lokupitiya, E., Luo, Y., Ma, S., Margolis, H., Matamala, R., McCaughey, H., Monson, R.K., Oechel, W.C., Peng, C., Poulter, B., Price, D.T., Riciutto, D.M., Riley, W., Sahoo, A.K., Sprintsin, M., Sun, J., Tian, H., Tonitto, C., Verbeeck, H., Verma, S.B., 2010. A model-data intercomparison of CO₂ exchange across North America: results from the North American carbon program site synthesis. *J. Geophys. Res.* 115, G00H05. <http://dx.doi.org/10.1029/2009JG001229>.
- Stoy, P.C., Katul, G.G., Siqueira, M.B.S., Juang, J.-Y., Novick, K.A., Uebelher, J.M., Oren, R., 2006. An evaluation of models for partitioning eddy covariance-measured net ecosystem exchange into photosynthesis and respiration. *Agric. For. Meteorol.* 141, 2–18. <http://dx.doi.org/10.1016/j.agrformet.2006.09.001>.
- Stull, R.B., 1988. *An Introduction to Boundary Layer Meteorology*. Springer, Netherlands, Dordrecht. <http://dx.doi.org/10.1007/978-94-009-3027-8>.
- Susaki, J., Yasuoka, Y., Kajiwara, K., Honda, Y., Hara, K., 2007. Validation of MODIS albedo products of paddy fields in Japan. *IEEE Trans. Geosci. Remote Sens.* 45, 206–217. <http://dx.doi.org/10.1109/TGRS.2006.882266>.
- Tang, X., Liu, D., Song, K., Munger, J.W., Zhang, B., Wang, Z., 2011. A new model of net ecosystem carbon exchange for the deciduous-dominated forest by integrating modis and flux data. *Ecol. Eng.* 37, 1567–1571. <http://dx.doi.org/10.1016/j.ecoleng.2011.03.030>.
- Tang, X., Wang, Z., Liu, D., Song, K., Jia, M., Dong, Z., Munger, J.W., Hollinger, D.Y., Bolstad, P.V., Goldstein, A.H., Desai, A.R., Dragoni, D., Liu, X., 2012. Estimating the net ecosystem exchange for the major forests in the northern United States by integrating MODIS and AmeriFlux data. *Agric. For. Meteorol.* 156, 75–84. <http://dx.doi.org/10.1016/j.agrformet.2012.01.003>.
- Tian, Y., Woodcock, C.E., Wang, Y., Privette, J.L., Shabanov, N.V., Zhou, L., Zhang, Y., Buermann, W., Dong, J., Veikkanen, B., 2002. Multiscale analysis and validation of the MODIS LAI product. *Remote Sens. Environ.* 83, 431–441. [http://dx.doi.org/10.1016/S0034-4257\(02\)00058-5](http://dx.doi.org/10.1016/S0034-4257(02)00058-5).
- Trotter, R.T., Morin, R.S., Oswalt, S.N., Liebhold, A., 2013. Changes in the regional abundance of hemlock associated with the invasion of hemlock woolly adelgid (*Adelges tsugae* Annand). *Biol. Invasions* 15, 2667–2679. <http://dx.doi.org/10.1007/s10530-013-0482-3>.
- Turner, D.P., Ritts, W.D., Cohen, W.B., Gower, S.T., Zhao, M., Running, S.W., Wofsy, S.C., Urbanski, S.P., Dunn, A.L., Munger, J.W., 2003. Scaling gross primary production (GPP) over boreal and deciduous forest landscapes in support of MODIS GPP product validation. *Remote Sens. Environ.* 88, 256–270. <http://dx.doi.org/10.1016/j.rse.2003.06.005>.
- Urbanski, S.P., Barford, C., Wofsy, S., Kucharik, C.J., Pyle, E., Budney, J., McKain, K., Fitzjarrald, D., Czikowsky, M.J., Munger, J.W., 2007. Factors controlling CO₂ exchange on timescales from hourly to decadal at Harvard forest. *J. Geophys. Res.* 112, G02020. <http://dx.doi.org/10.1029/2006JG000293>.
- van Ulden, A.P., 1978. Simple estimates for vertical diffusion from sources near the ground. *Atmos. Environ.* 12, 2125–2129. [http://dx.doi.org/10.1016/0004-6981\(78\)90167-1](http://dx.doi.org/10.1016/0004-6981(78)90167-1).
- Verma, M., Friedl, M.A., Law, B.E., Bonal, D., Kiely, G., Black, T.A., Wohlfahrt, G., Moors, E.J., Montagnani, L., Marcolla, B., Toscano, P., Varlagin, A., Rouspard, O., Cescatti, A., Arain, M.A., D'Odorico, P., 2015. Improving the performance of remote sensing models for capturing intra- and inter-annual variations in daily GPP: an analysis using global FLUXNET tower data. *Agric. For. Meteorol.* 214–215, 416–429. <http://dx.doi.org/10.1016/j.agrformet.2015.09.005>.
- Wang, Z., Schaaf, C.B., Lewis, P., Knyazikhin, Y., Schull, M.A., Strahler, A.H., Yao, T., Myneni, R.B., Chopping, M.J., Blair, B.J., 2011. Retrieval of canopy height using moderate-resolution imaging spectroradiometer (MODIS) data. *Remote Sens. Environ.* 115, 1595–1601. <http://dx.doi.org/10.1016/j.rse.2011.02.010>.
- Wehr, R., Saleska, S.R., 2015. An improved isotopic method for partitioning net ecosystem-atmosphere CO₂ exchange. *Agric. For. Meteorol.* 214–215, 515–531. <http://dx.doi.org/10.1016/j.agrformet.2015.09.009>.
- Welp, L.R., Randerson, J.T., Liu, H.P., 2007. The sensitivity of carbon fluxes to spring warming and summer drought depends on plant functional type in boreal forest ecosystems. *Agric. For. Meteorol.* 147, 172–185. <http://dx.doi.org/10.1016/j.agrformet.2007.07.010>.
- Woodcock, C.E., Strahler, A.H., Jupp, D.L.B., 1988a. The use of variograms in remote sensing. I - scene models and simulated images. II - real digital images. *Remote Sens. Environ.* 25, 323–348. [http://dx.doi.org/10.1016/0034-4257\(88\)90108-3](http://dx.doi.org/10.1016/0034-4257(88)90108-3).
- Woodcock, C.E., Strahler, A.H., Jupp, D.L.B., 1988b. The use of variograms in remote sensing: II. Real digital images. *Remote Sens. Environ.* 25, 349–379. [http://dx.doi.org/10.1016/0034-4257\(88\)90109-5](http://dx.doi.org/10.1016/0034-4257(88)90109-5).
- Wu, J., Larsen, K.S., van der Linden, L., Beier, C., Pilegaard, K., Ibrom, A., 2013. Synthesis on the carbon budget and cycling in a Danish, temperate deciduous forest. *Agric. For. Meteorol.* 181, 94–107. <http://dx.doi.org/10.1016/j.agrformet.2013.07.012>.
- Wu, Z.Y., Zhang, L., Wang, X.M., Munger, J.W., 2015. A modified micrometeorological gradient method for estimating O₃ dry deposition over a forest canopy. *Atmos. Chem. Phys. Discuss.* 15, 779–806. <http://dx.doi.org/10.5194/acpd-15-779-2015>.
- Xiao, X., Zhang, Q., Braswell, B.H., Urbanski, S.P., Boles, S., Wofsy, S.C., Moore, B., Ojima, D., 2004. Modeling gross primary production of temperate deciduous broadleaf forest using satellite images and climate data. *Remote Sens. Environ.* 91, 256–270. <http://dx.doi.org/10.1016/j.rse.2004.03.010>.
- Xu, K., Metzger, S., Desai, A.R., 2017. Upscaling tower-observed turbulent exchange at fine spatio-temporal resolution using environmental response functions. *Agric. For. Meteorol.* 232, 10–22. <http://dx.doi.org/10.1016/j.agrformet.2016.07.019>.
- Zhang, X., Friedl, M.A., Schaaf, C.L., Strahler, A.H., Hodges, J.C.F., Gao, F., Reed, B.C., Huete, A.R., 2003. Monitoring vegetation phenology using MODIS. *Remote Sens. Environ.* 84, 471–475. [http://dx.doi.org/10.1016/S0034-4257\(02\)00135-9](http://dx.doi.org/10.1016/S0034-4257(02)00135-9).